

1 **What controls fire size in the South American Gran Chaco?**
2 **Exploring atmospheric and landscape drivers through Remote**
3 **Sensing.**

4 Rodrigo San Martín¹, Catherine Ottlé¹, Anna Sorensön^{2,3,4}, Pradeebane Vaittinada Ayar¹,
5 Florent Mouillot⁵, Marielle Malfante⁶

6
7 ¹Laboratoire des Sciences du Climat et de l'Environnement, LSCE/IPSL, CEA-CNRS-UVSQ, Université Paris-
8 Saclay, Gif-sur-Yvette, France;

9 ²Centro de Investigaciones del Mar y la Atmósfera (CIMA), CONICET – Universidad de Buenos Aires, Buenos
10 Aires, Argentina;

11 ³CNRS, CNRS – IRD – CONICET – UBA, Instituto Franco-Argentino para el Estudio del Clima y sus Impactos
12 (IRL 3351 IFAECI), Argentina;

13 ⁴Facultad de Ciencias Exactas y Naturales, Universidad de Buenos Aires, Buenos Aires, Argentina;

14 ⁵UMR CEFE, University of Montpellier, CNRS, EPHE, IRD, Montpellier, France;

15 ⁶Univ. Grenoble Alpes, CEA, List, Grenoble, France;

16 *Correspondence to:* Rodrigo San Martin (rodrigo.sanmartin@lsce.ipsl.fr)

17

18 **Abstract.** Wildfires are key ecological agents in the Gran Chaco, one of the world's largest tropical dry
19 forest systems. We analyzed more than 100,000 fire patches across the Wet, Dry and Very Dry Chaco
20 between 2001 and 2022, to quantify environmental and anthropogenic controls on fire size. Fire sizes
21 were strongly right-skewed: more than 80 % were smaller than 5 km², yet large and extreme fires
22 dominated total burned area. Megafires (> 100 km²) occurred in all subregions, while gigafires (> 1000
23 km²) were rare but concentrated in the Dry Chaco. Fire Weather Index–burned area correlations
24 exhibited strong spatial contrasts, reaching values of up to $r = 0.7$ in the Wet Chaco and showing weaker,
25 more heterogeneous relationships in drier regions. Meteorological conditions during fires, particularly
26 persistent strong winds, were associated with larger and more elongated patches. Random Forest models
27 showed that topography and land cover composition together accounted for about 60 % of total SHAP
28 importance, whereas demographic variables had very low SHAP contributions in the models. Human
29 pressures shape ignition timing but showed limited direct influence on fire size once landscape structure
30 was included in the models. These results provide a quantitative basis for improving regional fire danger
31 assessments in the Gran Chaco.

32 1 INTRODUCTION

33 Wildfires shape global ecosystems by influencing vegetation structure, biodiversity, and landscape
34 composition (Bowman et al., 2009; Archibald et al., 2013; Chuvieco et al., 2020). The Gran Chaco,
35 spanning around 1.1 million km² across Argentina, Bolivia, Paraguay, and Brazil, is one of the largest
36 remaining dry forest ecosystems, with marked variation in precipitation, vegetation, and human land use
37 (Morello and Adámoli, 1968; Olson et al., 2001; Ginzburg et al., 2005; Torrella and Adámoli, 2005).
38 Fire has long modulated its vegetation structure and driven transitions between forests, shrublands, and
39 grasslands (Bucher, 1982; Kunst et al., 2003; Vidal-Riveros et al., 2023).

40 In recent decades, fire regimes in the Gran Chaco have shifted under the combined influence of land-
41 use intensification, changes in fire use and suppression practices, and increasing climatic variability
42 (Gasparri et al., 2008; De Marzo et al., 2021; Baumann et al., 2022; Marengo et al., 2022; Vidal-Riveros
43 et al., 2023; San Martín et al., 2023; San Martín, 2024).

44 Fuel characteristics and availability play a central role (Bravo et al., 2014; Argañaraz et al., 2016, 2018;
45 Vidal-Riveros et al., 2023). In native grasslands and savannas of the Gran Chaco, fine fuels typically
46 reach 4,000 to 5,000 kg of dry biomass per hectare per year, supporting medium to high intensity surface
47 fires (Bravo et al., 2025). In productive systems such as silvopastoral areas or improved pastures,
48 implanted tropical forage grasses can increase fine-fuel loads substantially (up to double the biomass),
49 locally enhancing fire intensity (Kunst et al., 2016).

50 Landscape heterogeneity further controls fire propagation, as the juxtaposition of rivers, wetlands,
51 shrublands, forests and grasslands in the Gran Chaco, together with traditional firebreak construction
52 and other local management practices, often restricts fire spread and creates natural or managed barriers
53 to fire (Kunst et al., 2003; San Martín et al., 2023; Vidal-Riveros et al., 2023; Bravo et al., 2025). These
54 interacting landscape controls challenge the idea of uniform and spatially consistent anthropogenic
55 effects on fire regimes across global dry ecosystems (Bistinas et al., 2014; Andela et al., 2017; Archibald
56 et al., 2018; Kelley et al., 2019; Jones et al., 2022).

57 Human activity is also a central component of fire regimes in the Gran Chaco. Across the region, most
58 ignitions originate from rural land management practices, including pasture renewal burns, garbage
59 burning, intentional clearing for agriculture or real-estate conversion, and opportunistic burning
60 associated with hunting (Naval Fernández et al., 2023; Vidal-Riveros et al., 2023; San Martín et al.,
61 2023; San Martín, 2024; Bravo et al., 2025). In the wetlands and floodplain grasslands of the Wet Chaco,
62 intentional burning for pasture renovation or vegetation clearing typically occurs towards the end of
63 winter and beginning of spring (end of the cold dry season) and, to a lesser extent, in late summer
64 (towards the end of the wet season) (San Martín et al., 2023). Winter burns are usually controlled and
65 produce small, patchy scars, whereas late-summer fires are more prone to escape and become larger,
66 particularly in anomalous dry years (Saucedo and Kurtz, 2025). Despite these differences in fire

67 behavior, vegetation often shows rapid post-fire recovery in the Wet Chaco (Bravo et al., 2025; Saucedo
68 and Kurtz, 2025). In contrast, the central and western Dry Chaco show a higher prevalence of land-
69 management fires linked to deforestation, rangeland conversion, and dry-season vegetation clearing
70 (Baumann et al., 2022; Gasparri et al., 2008; Naval Fernández et al., 2023; San Martín et al., 2023).
71 Between 2001 and 2019, nearly 40% of the 51.000 km² of deforested area in the Argentine Dry Chaco
72 was associated with burned surfaces (San Martín et al., 2023).

73 Cultural dimensions further contribute to the heterogeneity of ignition contexts across the Gran Chaco.
74 Fire use varies among actors, from small-scale subsistence cultivation in indigenous and rural
75 communities to larger-scale land clearing by commercial producers and private ranchers (Vidal-Riveros
76 et al., 2023). In parallel, indigenous wildfire narratives encode detailed ecological knowledge about fire
77 causes, behavior and post-fire recovery (Sugiyama et al., 2025), underscoring that fire is embedded in
78 diverse social and ecological understandings rather than representing a uniform anthropogenic pressure.
79 In this context, the 2020 fire season illustrated how socio-environmental factors interact under
80 exceptional circumstances. The COVID-19 pandemic altered mobility, enforcement capacity and on-
81 the-ground fire management across many regions worldwide. As discussed by Naval Fernández et al.
82 (2023), in several fire-prone landscapes, such as the Brazilian Pantanal and other tropical savannas, the
83 reduction or suspension of field surveillance and firefighting activities during lockdowns led to
84 increased fire activity (Garcia et al., 2021; Kumar et al., 2022; Eklund et al., 2022). In contrast, in other
85 regions, strict mobility restrictions reduced human-caused ignitions, highlighting the strong coupling
86 between human presence and fire occurrence, as reported for regions in Asia and North America
87 (Paudel, 2021; Poulter et al., 2021). In the Gran Chaco and adjacent drylands of central Argentina,
88 mobility also declined sharply during the peak fire months, yet suppression capacity remained relatively
89 stable due to the continued availability of volunteer brigades (Naval Fernández et al., 2023). Recent
90 socio-anthropological work further shows that the lockdown period through 2020 overlapped with
91 ongoing agrarian expansion and land-clearing dynamics, with deforestation, burning and road-
92 infrastructure projects proceeding despite mobility restrictions, reinforcing long-standing territorial
93 inequalities and weak institutional fire governance (Castilla, 2021; Schmidt and Castilla, 2023). This
94 combination indicates that many ignitions were not accidental or urban in origin, but instead linked to
95 rural land-clearing practices, pasture renewal and other management activities, underscoring the central
96 role of human agency even under atypical social conditions (Naval Fernández et al., 2023; San Martín,
97 2024).

98 At broader temporal and spatial scales, climatic variability, especially the occurrence of prolonged
99 droughts related to the intensification of episodes of multi-year strong El Niño–Southern Oscillation
100 (ENSO) negative phases (La Niña), has been associated with large fire seasons in the Chaco and
101 neighboring biomes (Alencar et al., 2015; Naumann et al., 2023). These climate anomalies reduce fuel
102 moisture and extend the window for fire spread (Doblas-Reyes et al., 2021; De Marzo et al., 2023; Arias
103 et al., 2024). In particular, several recent extreme fire seasons coincided with the 2020–2023 La Niña,

104 which strongly affected moisture availability and fire activity throughout the Gran Chaco and its
105 surroundings (Kumar et al., 2022; Naval Fernández et al., 2023; San Martín, 2024).

106 Although individual drivers of fire occurrence are increasingly well understood, the way these factors
107 interact to determine the final size of fires in the Gran Chaco remains poorly quantified. Existing studies
108 highlight the importance of drought, fuel moisture deficits and human land use in shaping ignition
109 patterns and BA totals, yet the mechanisms that control how far fires spread under contrasting
110 environmental and land-use contexts remain unresolved (San Martín et al., 2023; Vidal-Riveros et al.,
111 2023, 2024; Bravo et al., 2025). Baumann et al. (2022) showed that deforestation pathways vary by actor
112 and context, altering fuel configurations and fire–landscape interactions, San Martín et al. (2023)
113 demonstrated that precipitation–BA relationships differ markedly across land-cover types, and Levers
114 et al. (2024) projected that continuing agribusiness expansion could intensify fire impacts on
115 ecologically and socially sensitive areas. Together, these studies reveal substantial spatial heterogeneity
116 in fire dynamics, but none explicitly evaluate how meteorological variability interacts with landscape
117 structure and human pressures to shape final fire size.

118 Some classification efforts have begun to map regional fire diversity but still overlook key atmospheric
119 determinants. Vidal-Riveros et al. (2024) grouped Paraguayan Chaco fire regimes by severity, frequency
120 and extent, while Naval-Fernández et al. (2025) used multivariate clustering of landscape attributes to
121 delineate pyroregions in the Argentine Chaco. These approaches captured meaningful spatial patterns,
122 yet they did not incorporate high-resolution meteorological conditions, limiting their ability to identify
123 the atmospheric processes that influence fire expansion.

124 In summary, no study has yet combined meteorological anomalies, fire morphology metrics, and
125 landscape context to assess how short-term weather and long-term environmental gradients determine
126 fire size in the Gran Chaco. This gap is critical given the biome's diverse ignition sources, propagation
127 through heterogeneous fuels, and sharp transitions in hydrology, vegetation structure, and land-use
128 intensity.

129 Advances in satellite Earth Observation now allow for such integration. Global burned area (BA)
130 products such as FireCCI51 offer consistent daily burned surface estimates at moderate spatial resolution
131 (Chuvieco et al., 2020). Event-based datasets including FRY (Laurent et al., 2018; Mouillot et al., 2023)
132 and the Global Fire Atlas (Andela et al., 2019) reconstruct individual fires and enable the analysis of
133 attributes such as ignition date, duration, size and morphology (Moreno et al., 2021; Takacs et al., 2021;
134 García et al., 2022). In this study, we use FRYv2.0, which integrates the FRYv1.0 pixel aggregation
135 method with the latest version of FireCCI51 BA mapping (Lizundia-Loiola et al., 2020), and we
136 combine it with environmental and meteorological datasets to quantify how different drivers influence
137 fire size across the Gran Chaco.

138 Specifically, we aim to answer the following scientific questions:

139 (1) What are the primary fire-size characteristics and their frequency across the Gran Chaco between
140 2001 and 2022? (2) To what extent do meteorological conditions influence the size and expansion of

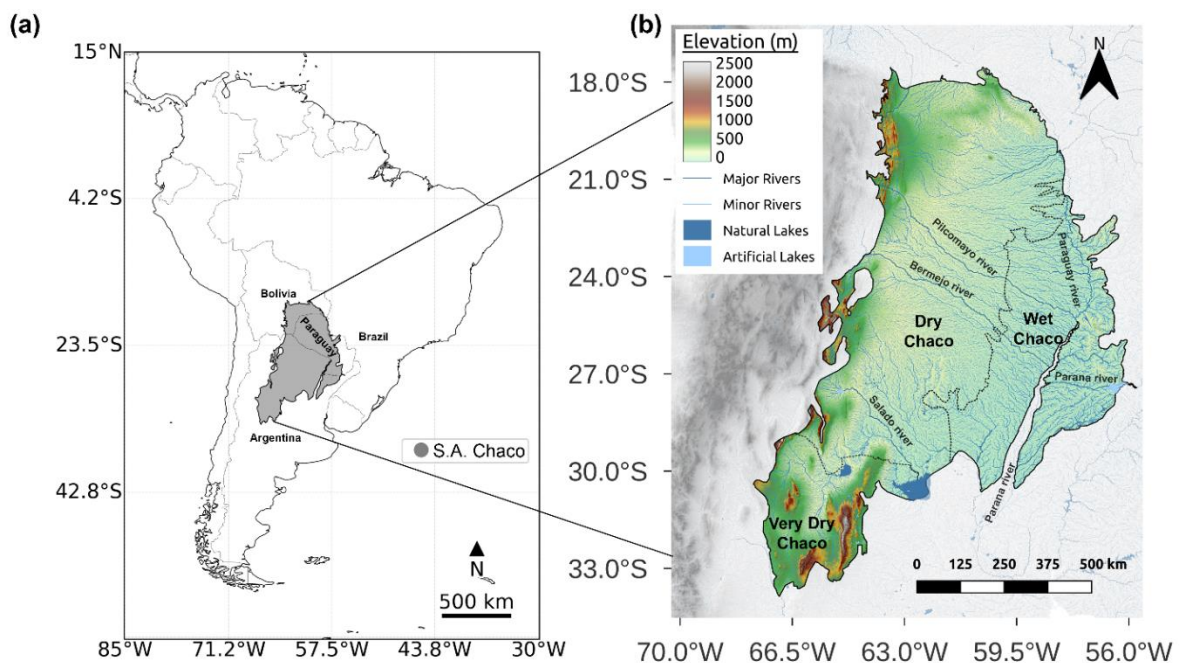
141 individual fires? (3) Beyond weather, what roles do vegetation type, topography and human activity
142 play in shaping fire size and fire occurrence across the region? (4) Which of these drivers best explain
143 the spatial and temporal variability of fire size among the different subregions of the Gran Chaco?

144 **2 METHODS**

145 **2.1. Study area**

146 The Gran Chaco is an extensive tropical and subtropical region of South America, covering
147 approximately 1,100,000 km² (**Fig. 1**). It contains the world’s largest continuous dry tropical forest and
148 extensive wetland systems (Bucher, 1982; Olson et al., 2001). In the literature, terminology varies with
149 references to the South American Chaco, the Gran Chaco, or just Chaco. To avoid confusion, we only
150 use Gran Chaco in this work.

151



152 **Fig. 1.** The Gran Chaco location in South America (a) and its topography (b) with its different subregions, main rivers, and lakes. Based on
153 Shuttle Radar Topography Mission (SRTM) at 90m (SRTM | NASA Earthdata, 2024) and HydroSHEDS (Lehner et al., 2008).
154

155
156 The region is mostly flat and low (<200 m), with higher and undulating terrain towards the northeast
157 limit (up to ~500 m), the western Andean foothills (up to ~2,000 m), and the southwestern Sierras de
158 Córdoba (reaching 2,790 m at Mt. Champaquí). Following Olson et al. (2001), we delimit a humid
159 eastern Wet Chaco from a drier western Dry Chaco, structured along marked west–east gradients in
160 precipitation, vegetation, and hydrology (Morello and Adámoli, 1968; Bucher, 1982; Ginzburg et al.,
161 2005; Torrella and Adámoli, 2005). Following Baumann et al. (2018), we further identify a drier
162 southwestern subregion referred to as the Very Dry Chaco, characterized by lower biomass, greater
163 aridity, higher elevations, and distinct fire regimes. Its extent is delimited by the Argentine provincial
164 borders of Mendoza, San Luis, Córdoba, San Juan, and La Rioja.

165 For the 2001–2020 period, mean annual precipitation averaged approximately 600 mm/year in the Very
166 Dry Chaco, 860 mm/year in the Average Dry Chaco, and 1,375 mm/year in the Wet Chaco, with local

167 maxima in the eastern sector approaching 1,800 mm/year (San Martín et al., 2023; San Martín, 2024).
168 These precipitation differences are reflected in contrasting land-cover structures: the Wet Chaco
169 includes extensive wetlands, floodplains, grasslands, and palm savannas; the Average Dry Chaco is
170 dominated by drought-adapted forests and shrublands increasingly interspersed with agricultural fields;
171 and the Very Dry Chaco is characterized by more open shrublands and dry forest patches.
172 Regarding its hydrology, the Gran Chaco forms part of the La Plata basin (Barros et al., 2006; Musser,
173 2024). Rivers such as the Pilcomayo, Bermejo, and Salado originate in the Andes, cross the Dry Chaco,
174 and disperse into alluvial megafans, streams, and wetlands in the eastern Wet Chaco. This west–east
175 hydrological gradient drives seasonal contrasts: in dry months, the Dry Chaco faces water scarcity,
176 whereas the Wet Chaco retains permanent wetlands that sustain ecological processes and fauna (Cabrera,
177 1976; Bucher, 1982; San Martín, 2024). Additionally, the region harbors exceptional biodiversity, with
178 over 3,400 plant species and hundreds of vertebrates, many endemic (Redford et al., 1990; Bucher and
179 Huszar, 1999; Nori et al., 2016).
180 Fire activity shows pronounced subregional contrasts across the Gran Chaco. The Wet Chaco presents
181 a bimodal fire season, with peaks at the end of the warm wet season (late summer–autumn) and again at
182 the end of the cold dry season (late winter–spring), while the Dry Chaco exhibits a unimodal pattern
183 restricted to the end of the cold dry season, towards late winter–spring (Kunst and Bravo, 2003; Bravo
184 et al., 2010, 2025; San Martín et al., 2023). Mean annual BA is about 15,000 km²/yr in the Wet Chaco
185 and roughly 8,500 km²/yr in the Dry and Very Dry Chaco together, based on annual BA totals for 2001–
186 2019. Despite its higher annual BA, much of the Wet Chaco burns repeatedly, with ~57% of its burned
187 surface experiencing at least two fire events between 2001 and 2019. In contrast, about 66% of the
188 burned surface in the Dry Chaco represents one-time fires, with burns advancing over previously
189 unburned forests. In this western subregion, fires typically follow deforestation rather than acting as the
190 primary clearing mechanism (San Martín et al., 2023). These contrasts reflect the greater continuity of
191 fine fuels and higher fire recurrence in the eastern Wet Chaco, compared with the more intermittent and
192 fuel limited conditions characterizing the Dry and Very Dry Chaco.

193

194 **2.2 Datasets**

195 2.2.1 Fire patches

196 In this study, we used FRYv2.0, a recent global database of fire patch (FP) functional traits (morphology,
197 fire spread, and timing) to investigate fire dynamics and their underlying drivers in the Gran Chaco
198 (Laurent et al., 2018; Mouillot et al., 2023). FRYv2.0 is an updated, second-generation version of the
199 original FRY database that aggregates burned area (BA) pixels from the latest FireCCI51 dataset and
200 from the MODIS MCD64A1 product into individual FPs using fixed temporal cut-offs of 6, 12, or 24
201 days to delimit the extent of a fire event or the onset of a new one. Compared with the original release,
202 it provides extended patch-level information, including morphology (for example area, perimeter, shape

203 index, core area), temporal traits such as burn dates and duration, dynamic traits such as rate of spread,
204 fire radiative power (FRP) and severity indicators, and associated land cover. The FRYv2.0
205 morphological metrics describe the geometry and structure of each FP: *n_cell* quantifies the number of
206 burned pixels from the input BA product that form the fire patch; area represents the total burned surface;
207 the *shape index* captures deviations from a compact circular shape; the *core-area index* indicates the
208 proportion of interior, non-edge area; *eccentricity* measures patch elongation; and the *perimeter-to-area*
209 *ratio* characterizes boundary complexity and compactness.

210 Patch-level functional traits are computed only for patches composed of at least five burned pixels, to
211 avoid geometric and orientational instability in very small patches. FRP-based diagnostics, including
212 ignition timing derived from active-fire detections, are assigned only to patches larger than 100 ha
213 (approximately sixteen FireCCI51 pixels). This ignition dating offers a more accurate estimate of fire
214 onset than the default burn-date information in FireCCI51 or MODIS MCD64A1, which relies on the
215 day of first BA detection.

216 For this work, we selected the FRYv2.0 version based on FireCCI51 rather than the version based on
217 the MODIS MCD64A1 BA product, because the FireCCI51 input has higher spatial resolution (250 m
218 compared to 500 m), provides better spatial detail for the heterogeneous landscapes of the Gran Chaco,
219 and ensures consistency with our previous FireCCI51 based analysis (San Martín et al., 2023), thus
220 avoiding additional uncertainty from mixing BA products. The FRYv2.0 FireCCI51-based dataset used
221 here is publicly available at <https://osf.io/rjvz5/files/osfstorage> (last accessed on 10 June 2025).

222 2.2.2 Meteorological Data

223 To study meteorological and climate time series in the region, we used the ERA5-Land global reanalysis
224 dataset focused on land surface variables, developed by the European Centre for Medium-Range
225 Weather Forecasts (ECMWF) (Muñoz-Sabater et al., 2021). It provides high-resolution data for land–
226 atmosphere interactions, designed to improve the ERA5 dataset by offering finer detail (0.1° instead of
227 0.25° spatial resolution) for variables affecting the land surface.

228 The product is available in the Copernicus Data Store (CDS) in NetCDF at
229 <https://cds.climate.copernicus.eu/cdsapp#!/dataset/reanalysis-era5-land> (last accessed on 30 May 2024).

230 We downloaded hourly data arrays covering January 2001 through January 2023.

231

232 2.2.3 Environmental and Anthropogenic Data

233 We compiled several spatial datasets that represent biophysical conditions and human-related drivers
234 relevant to fire activity in the Gran Chaco.

235 *Topography* was obtained from the NASA SRTM v3 product (<https://srtm.csi.cgiar.org>, accessed 26
236 May 2025). This product provides a 3 arc-second (approximately 90 m) digital elevation model (DEM)
237 in WGS84 geographic coordinates. Slope and aspect were calculated from this DEM using the Horn

238 algorithm as implemented in the *richdem TerrainAttribute* function, which estimates local gradients
239 over 3 by 3 cells (Horn, 1981).

240 *Land cover* (LC) was obtained from the ESA Climate Change Initiative Moderate Resolution Land
241 Cover product (CCI MRLC; <https://cds.climate.copernicus.eu/datasets/satellite-land-cover>, accessed 26
242 May 2025). This product provides annual maps at 300 m spatial resolution for the period 1992 to 2022.
243 We selected CCI MRLC because its resolution is appropriate for the regional extent of this study, which
244 covers more than 1,100,000 km². The product has undergone extensive validation, is widely used in
245 regional land surface studies, and ensures consistency with our previous analyses in the Gran Chaco
246 (Defourny et al., 2023; Harper et al., 2023; San Martín et al., 2023).

247 *Fuel accumulation* before each fire was characterized using MODIS LAI at 500 m resolution and 8-day
248 intervals. We used MOD15A2H (Terra) for 2001 to 2002 and MCD15A2H (Terra and Aqua combined)
249 for 2002 to 2023. Only observations with quality level 0 were retained. For each fire, we extracted all
250 LAI values from MODIS pixels that overlapped the fire patch. To represent the accumulated biomass
251 that could contribute to fire spread, we defined the pre-fire period as the interval between 1 August of
252 the year before the fire and the ignition date. This window captures the seasonal minimum at the end of
253 the winter dry season and the entire subsequent growing season. A 4-step rolling mean with a minimum
254 of one valid value was applied to reduce high frequency noise. The final pre-fire LAI value for each fire
255 patch was the mean LAI across this August to ignition interval. This variable, which we refer to as the
256 mean LAI of the previous growing season, served as a proxy for the biomass accumulated before the
257 fire.

258 *Soil properties* were obtained from the SoilGrids250m database. The variables used were soil organic
259 carbon at 0 to 5 cm depth, sand fraction, and bulk density. We used the one-kilometer aggregated layers
260 provided by *SoilGrids* and computed means for each fire patch.

261 *Population density* was taken from the Gridded Population of the World version 4 (GPWv4) (CIESIN,
262 2017; <https://www.earthdata.nasa.gov/data/projects/gpw>, accessed November 25, 2025). The native
263 resolution of this product is approximately 30 km. Since the dataset was not modified, population values
264 were assigned to each fire patch using nearest neighbor extraction.

265 *Livestock density* was obtained from the Gridded Livestock of the World version 4 (GLWv4;
266 https://dataverse.harvard.edu/dataverse/glw_4, accessed November 25, 2025). This dataset is available
267 at roughly 10 km resolution. The original values were used as provided. For each fire patch, livestock
268 density (number of cattle / km²) was summarized using zonal means.

269 *Road density* was derived from two global road network datasets to account for uncertainties in road
270 mapping, particularly the incomplete representation of informal, unpaved or irregular roads in some
271 regions of the Gran Chaco. We used two independent sources: OpenStreetMap (OSM;
272 <https://www.openstreetmap.org>, accessed November 25, 2025), which is community-curated and
273 generally more complete in populated areas, and the Microsoft Bing AI Global Roads dataset (MS;
274 <https://github.com/microsoft/RoadDetections>, accessed November 25, 2025), which is algorithmically

275 extracted from high-resolution satellite imagery and tends to provide broader coverage in rural and
276 sparsely populated landscapes. For all main analyses, road density was computed from the OSM dataset,
277 while the MS product was used only in a sensitivity experiment to evaluate the robustness of road-
278 related effects (see *Section 2.3.9*).

279 Roads were maintained in vector format and intersected with a regular 0.03° grid (~3 km), projected
280 onto an equal-area coordinate system for accurate calculations of road length and cell area. Road density
281 (km km⁻²) was computed for each grid cell, and fire patches were assigned an area-weighted mean value
282 based on all overlapping cells. The 0.03° resolution was selected after testing coarser and finer grids,
283 providing the best trade-off between capturing road density within each patch and preserving the
284 surrounding spatial context while maintaining consistency across both road datasets. Using both
285 products in this way ensured that the inferred influence of human accessibility on fire behavior was not
286 dependent on a single mapping dataset, while keeping OSM as the reference road layer for the core RF
287 configurations.

288 2.2.3 Climate Oscillations

289 To account for the influence of large-scale climate variability, we included the Multivariate El Niño–
290 Southern Oscillation (ENSO) Index version 2 (MEI.v2), developed by NOAA's Physical Sciences
291 Laboratory. The MEI.v2 time series was obtained from NOAA PSL at <https://psl.noaa.gov/enso/mei/>
292 (last accessed 26 May 2025).

293

294 **2.3 Data processing and analysis methods**

295 2.3.1 Fire Weather Index (FWI)

296 We built an ERA5-Land-based Canadian Fire Weather Index (FWI; Van Wagner, 1987) dataset for the
297 Gran Chaco at 0.1° resolution and daily time steps. We converted hourly accumulated precipitation to
298 hourly rainfall by differencing successive steps and summing totals from 15 UTC (day D-1) to 15 UTC
299 (day D), matching the FWI daily window and corresponding to local noon in most of the Gran Chaco.
300 We applied this fixed 15 UTC cutoff to the full region to avoid inconsistencies caused by varying
301 national time zones and daylight-saving changes.

302 We extracted daily meteorological inputs (i.e., air temperature, relative humidity, wind speed at local
303 noon, and 24-h precipitation) to compute the six FWI sub-indices: Fine Fuel Moisture Code (FFMC),
304 Duff Moisture Code (DMC), Drought Code (DC), Initial Spread Index (ISI), Build-Up Index (BUI), and
305 FWI. We performed calculations with an adapted version of the *FireDanger* Python package
306 (<https://github.com/steidani/FireDanger>) compatible with *xarray* and *NetCDF*, including pixel-level day
307 length for DMC and hemisphere-specific drying factors for DC. We initialized the system on 1 January
308 1981 using Copernicus ERA5–FWI moisture codes at 0.25° (Vitolo et al., 2020) interpolated to 0.1°.

309 2.3.2 Land Cover processing

310 For this work, the original classes of CCIMRLC were grouped into eight categories relevant to the Gran
311 Chaco fire regime. These categories included tree cover, shrublands, grasslands, seasonally flooded
312 herbaceous vegetation, croplands, two mixed mosaics containing combinations of herbaceous and
313 woody vegetation, and an extra class we called “Others”, grouping the remaining underrepresented
314 classes in the Gran Chaco. For each FP we extracted the fractions of LC at the year of fire ignition, and
315 these fractions were used to calculate the following landscape heterogeneity indices:

316 In order to quantify the landscape heterogeneity within each FP and assess how the mix and spatial
317 balance of LC types influence fire outcomes, we calculated the Shannon diversity index (H) and Pielou's
318 evenness (E). They were computed as follows:

319

320 **(Eq. 1)** Shannon Diversity Index (Shannon, 1948):

321
$$H = - \sum_{i=1}^m p_i \log(p_i)$$

322 Where m is the number of land cover classes present in the fire patch, p_i is the proportion of land cover
323 type i , and the sum includes all classes with $p_i > 0$.

324

325 **(Eq. 2)** Pielou's evenness (Pielou, 1966):

326
$$E = \frac{H}{\log(m)}$$

327 Where H is the Shannon Diversity Index and m is the number of land cover classes present in the fire
328 patch.

329

330 2.3.3 Wind indices

331 Using ERA5-Land data, we calculated for each FP a metric specifically designed to capture the role of
332 strong, persistent winds in shaping fire behavior: the Extreme Wind Directionality Index
333 (EW_dir_index). This index measures both how often extreme winds occurred and how steady their
334 direction was.

335 The first component, fraction of extreme-wind days (EW_frac), is the proportion of burning days when
336 the daily maximum wind speed exceeded 25 km h^{-1} :

337 **(Eq. 3)** Extreme Wind Fraction Index:

338
$$EW_frac = \frac{EW}{N}$$

339 where EW is the number of days with extreme winds and N is the total fire duration (days). High values
340 indicate that strong winds occurred on many burning days.

341 The second component, wind direction steadiness ($wind_dir_R$), reflects how consistent the wind
342 direction was across the fire’s duration (N). Each day’s mean wind direction (θ_i , in radians) is
343 represented as a unit vector, summed across all days, and normalized by the fire duration:

344 **(Eq. 4)** *Wind Directionality Index:*

$$345 \quad wind_dir_R = \frac{\sqrt{(\sum_{i=1}^N \cos \theta_i)^2 + (\sum_{i=1}^N \sin \theta_i)^2}}{N}$$

346 Values near 1 mean that winds blew in a stable direction throughout the event, while values near 0 mean
347 that wind directions shifted substantially from day to day.

348 The EW_dir_index is the product of EW_frac and $wind_dir_R$:

349 **(Eq. 5)** *Extreme Wind Directionality Index:*

$$350 \quad EW_dir_index = EW_frac \times wind_dir_R$$

351 It reaches high values only when strong winds occur on many burning days and blow consistently from
352 the same direction, identifying fires likely driven by sustained, unidirectional wind conditions.

353 2.3.4 Burned Area vs Fire Counts

354 To examine the interannual relationship between fire counts and total BA, we compared annual BA and
355 annual fire counts for each of the three Gran Chaco subregions using FRYv2.0. For every year in 2001–
356 2022, total BA was computed as the sum of the burned surface of all fire patches within each subregion,
357 while fire counts were obtained as the number of individual patches whose ignition date fell within that
358 year. We then fitted simple linear regressions between annual BA and annual fire counts for each
359 subregion to quantify how ignition frequency explains interannual variability in BA and to assess
360 whether this relationship differs among the subregions and between the wet and dry seasons.

361 2.3.5 Fire size classification

362 To examine how fires of different magnitudes contribute to overall fire activity in the Gran Chaco, we
363 classified all FRYv2.0 fire patches (FPs) into six size categories. Fire events can be grouped according
364 to various criteria, including behavior (e.g., rate of spread, intensity), ecological impact (e.g., severity),
365 structural properties (e.g., shape, perimeter), or final extent (total burned area). Because our objective is
366 to identify the determinants of final fire size, we adopted a size-based classification. This approach
367 directly aligns the categorization with the response variable and facilitates interpretation of the climatic,
368 landscape, and anthropogenic drivers controlling it.

369 To avoid ad-hoc or region-specific thresholds, we followed the standardized fire-size typology proposed
370 by Linley et al. (2022), who conducted the first global assessment aimed at harmonizing terminology
371 for large fires. They argue that terms such as “*megafire*” or “*large wildfire*” had been used inconsistently
372 across disciplines and agencies, often referring to different orders of magnitude depending on national
373 contexts or management traditions. They show that this lack of standardization complicates cross-
374 regional comparison and the interpretation of extreme events. To resolve this, they propose clear, size-

375 based definitions applicable worldwide: megafires as events with BA > 10,000 ha (100 km²), gigafires
376 > 100,000 ha (1000 km²), and terafires > 1,000,000 ha (10,000 km²). Their framework is explicitly
377 designed for satellite-derived BA products, including those used to build FRY, and provides a consistent
378 basis for global and regional analyses.

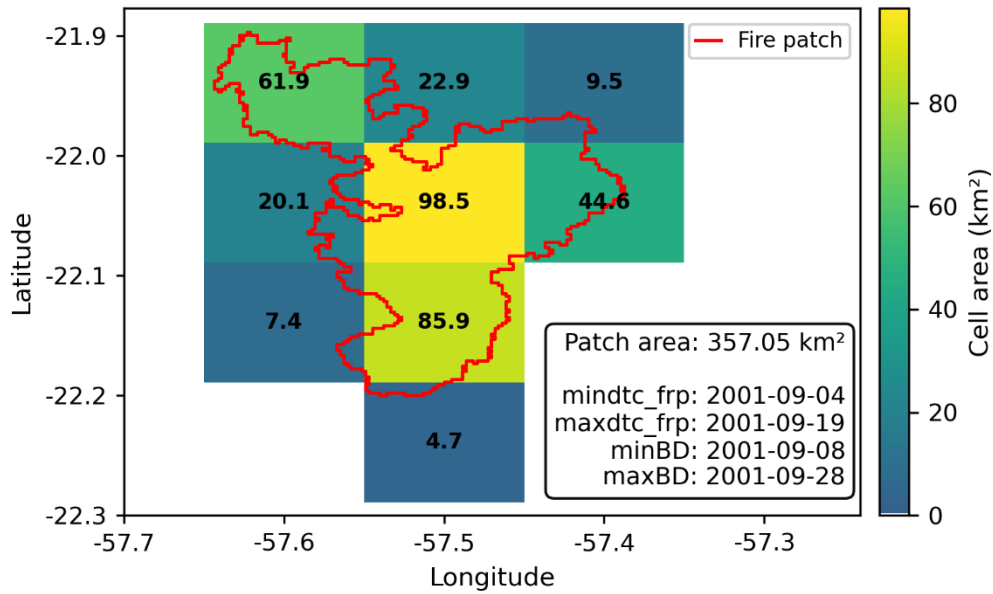
379 Using Linley's typology ensures that extreme fire classes in the Gran Chaco are comparable to global
380 assessments and avoids relying on operational thresholds used in some countries (e.g., 40,000 ha) that
381 lack a physical or ecological rationale. At the same time, the empirical distribution of FRYv2.0 patch
382 sizes in the Chaco is strongly right-skewed, with most events being small and only a few exceeding the
383 megafire threshold. For this reason, and to retain regional relevance, we added to Linley's standardized
384 thresholds four smaller size classes suitable for the Gran Chaco, while preserving the key cut-offs at 100
385 km² and 1000 km². FRYv2.0 imposes a practical lower limit on measurable patch size: functional traits
386 are computed only for patches composed of at least five FireCCI51 pixels (~0.3 km²), and FRP-based
387 diagnostics, including ignition dating, are provided only for patches larger than ~100 ha (1 km²; see
388 *Section 2.2.1*). This naturally defines the smallest reliable category in our system.

389 The resulting scheme spans from a "very small" class (0–1 km²), which is more uncertain because FRY
390 patches in this range often lack complete geometric or FRP-based diagnostics, through small (1–5 km²),
391 medium (5–10 km²), and large (10–100 km²) events, up to megafires (100–1000 km²) and gigafires
392 (>1000 km²). No fire in the Gran Chaco exceeded 10,000 km², and therefore the terafire class defined
393 by Linley et al. is not used in this work.

394 2.3.6 Gridded burned area

395 To enable a spatiotemporal comparison between fire activity from FRYv2.0 fire patches and
396 meteorology, we developed a pipeline to transform the FP-based data into a monthly gridded product at
397 0.1°, matching the ERA5-Land grid (**Fig. 2**).

398



399

400 **Fig. 2.** Example of one FRY fire patch (red line) over the gridded FRY dataset. Each grid cell at 0.1° is assigned the burned area corresponding
 401 to the total fraction of the patch that overlaps it. The values printed over each grid cell correspond to these values.
 402

403 The temporal assignment of fires to months followed a hybrid strategy: where MODIS-derived hotspot
 404 detection dates (*mindtc_frp* and *maxdtc_frp*) were available in a given FP (typically absent in very small
 405 FPs) they were used. Both FireCCI51- and MODIS-based versions of FRYv2.0 include these hotspot
 406 date variables when available for the FP. When hotspot dates were missing, we used the FireCCI51-
 407 derived burn dates (*minBD* and *maxBD*), which are based on surface reflectance changes and are
 408 available for all FPs. For FPs spanning multiple months, we assigned the fire to the month in which it
 409 started, unless its duration in a subsequent month exceeded that of the starting month by more than two
 410 days.

411 Each FP was rasterized on a 0.01° grid by intersecting it with individual cells. The intersected area in
 412 square kilometers was computed using the WGS84 ellipsoid model. These contributions were
 413 aggregated per cell and per assigned month to build a three-dimensional array of monthly BA (*lat x lon*
 414 *x time*). A similar procedure was implemented for fire counts, using ignition (first detection) coordinates
 415 and dates. Each FP's fire ignition coordinate was allocated to the closest cell in the 0.1° grid. The
 416 resulting monthly gridded dataset included two variables: BA and counts.

417 To compute monthly BA anomalies, we derived pixel-level monthly climatologies for the period 2001–
 418 2020 from the gridded BA dataset. Anomalies were defined as the difference between each monthly BA
 419 value and the corresponding monthly climatological mean, following the same temporal normalization
 420 applied to meteorological variables.

421

422 2.3.7 Anomalies and climatologies

423 For all ERA5-Land variables, as well as the FWI index and its sub-indices, we computed pixel-level
424 daily climatologies using the 2001–2020 mean as the baseline. Meteorological anomalies were then
425 defined as the daily deviation from this climatology and subsequently aggregated to monthly values to
426 match the temporal scale of the BA analysis.

427 To compute monthly BA anomalies, we derived pixel-level monthly climatologies for the period 2001–
428 2020 from the gridded BA dataset. Anomalies were defined as the difference between each monthly BA
429 value and the corresponding monthly climatological mean, following the same temporal normalization
430 applied to meteorological variables. This anomaly-based formulation was used only for the correlation
431 analysis with FWI anomalies and not for any other statistical or spatial analyses in the manuscript.

432 For the specific analysis comparing monthly BA anomalies with monthly FWI anomalies, only pixels
433 with at least four fire-active months ($BA > 0$) during 2001–2022 were retained to avoid artefacts from
434 sparsely populated or highly skewed anomaly series. Correlations were computed using both Pearson’s
435 coefficient and Spearman’s rank coefficient.

436 We did not apply an FWI95-based threshold or similar fixed-percentile metrics, as these are less
437 comparable across the strong climatic gradient of the Gran Chaco and may artificially amplify or
438 dampen fire–weather relationships depending on local baseline conditions. Using pixel-level anomalies
439 instead allows each location to be evaluated relative to its own climatology, yielding a spatially
440 consistent and locally meaningful basis for comparison.

441

442 2.3.8 Fire-weather types

443 We classified fire patches (FPs) into three groups based on associated atmospheric conditions using the
444 K-means clustering algorithm (MacQueen, 1967) in *Python’s scikit-learn v1.3*. This approach follows
445 prior applications in fire studies (Ruffault et al., 2016, 2020; Vidal-Riveros et al., 2024) and aimed to
446 identify distinct fire-weather types (FWTs) and assess their influence on fire size and shape.

447 For this clustering analysis, we retained only fire patches between 1 and 100 km² ($N = 78,052$). At the
448 lower end, this choice is consistent with the construction of the FRYv2.0 database, where the FP
449 functional traits are computed only for patches composed of at least five burned pixels and smaller
450 patches are filtered out because their geometry and orientation are considered unreliable (see *Section*
451 *2.2.1*). In addition, FRP based diagnostics, including ignition timing derived from active fire detections,
452 are only provided for FPs larger than 1 km² (approximately 16 FireCCI51 pixels), so the smallest events
453 lack both robust geometric traits and FRP timing information. At the upper end, fires larger than 100
454 km² were excluded from the K-means analysis. In addition to their low frequency, these very large, long
455 duration patches often span heterogeneous landscapes and experience several distinct weather situations
456 over their burning period, so the associated ERA5-Land and FWI time series mix conditions from distant
457 locations and different days. This mixing makes the patch-averaged meteorological descriptors difficult

458 to interpret as a single coherent FWT and would likely introduce substantial biases in the clustering and
459 in the Random Forest (RF) models used later to analyze fire size drivers (see *Section 2.3.9*).
460 For each FP within the 1–100 km² range, we extracted daily ERA5-Land meteorological data and the
461 computed FWI time series from 7 months before ignition to 7 months after, and then built two feature
462 sets, one representing pre-fire conditions and one representing conditions during the fire.
463 For the *Pre-Fire* set, we used normalized anomalies of 2-m air temperature, 10-m wind speed, relative
464 humidity (RH), drought code (DC), and duff moisture code (DMC) (Ruffault et al., 2020). Pre-fire
465 values were calculated as the 3-day mean from ignition day (D) to D-2 to limit detection-date bias
466 (Lizundia-Loiola et al., 2020; Pettinari et al., 2021) while avoiding noise from longer lags.
467 For the *During-Fire* set, we computed the same variables averaged over the fire’s duration and added
468 the *Extreme Wind Fraction Index* and the *Extreme Wind Directionality Index*, described in *Section 2.3.3*.
469 All variables in both sets were standardized before clustering (mean = 0, $\sigma = 1$). The resulting data
470 matrix was clustered with $k = 3$, squared Euclidean distance, *k-means++* initialization, 50 random
471 restarts, and a convergence tolerance of 10^{-4} . We retained three clusters based on a prior hypothesis
472 (wind-driven, drought-driven, and neutral), an elbow in the within-cluster sum-of-squares curve, and a
473 peak in the silhouette coefficient at $k = 3$.
474 Cluster labels were assigned by interpreting centroid positions in principal component space and
475 examining the temporal evolution of variables (**Fig. S1**). Robustness was assessed using mean silhouette
476 coefficients and their distribution across clusters. The first two principal components explained more
477 than 60 % of the variance and clearly separated cluster centroids.

478

479 2.3.9 Fire size drivers

480 To investigate the role of environmental and anthropogenic variables in determining fire size, we
481 extracted a diverse set of FP-level potential predictors encompassing topographic, climatic,
482 anthropogenic, vegetation, and landscape heterogeneity dimensions. These variables, listed in **Table 1**,
483 were used as inputs in the RF models to assess their relative importance in explaining fire size.

484 Once all potential predictor variables were derived, we trained RF models using a set of 17 explanatory
485 variables to analyze the drivers of fire behavior, using the variable *n_cell* from the FRY dataset as the
486 response variable. This variable represents the number of FireCCI51 pixels within each FP and was
487 preferred over patch-based *area* due to the latter’s dependency on latitude, which introduced artificial
488 discontinuities. In contrast, *n_cell* provided a discrete and spatially consistent proxy for BA, improving
489 model stability and interpretability.

490 We implemented 12 primary RF models across five configurations: (i) a global model using all the
491 78,052 fire patches used for the clustering analysis (patches with area between 1 and 100 km²), (ii) three
492 subregion-specific models for the Wet, Dry, and Very Dry Chaco, (iii) two seasonal models based on

493 ignition season (wet vs dry), and (iv) two sets of three cluster-based models (pre-fire and during-fire
 494 conditions) derived from the FWT classification (see *Section 2.3.8*).

495

496 **Table 1.** Target and potential predictor features extracted from each FRY fire patch within the Gran Chaco region, grouped by variable types.
 497 These features were used for the Random Forest models trained in this work.

Category	Variables
Fire Size (target feature)	Number of pixels within the fire patch (250 m pixels from FireCCI51)
Topography	Mean Slope (%) Mean Elevation (m)
Meteorology (during fire mean)	Precipitation (mm) Maximum Wind Speed (km/h) Extreme Wind and Direction Index (EW_dir_index) Extreme Wind Days Fraction (EW_frac)
Anthropogenic proxies (year of fire ignition)	Cattle Density (heads/km ²) Road Density (km/km ²) Population Density (p/km ²)
Vegetation productivity (previous growing season)	LAI for previous growing season (MODIS-derived)
Land Cover Composition (year of fire ignition)	Flooded Herbaceous vegetation (%) Tree Cover (%) Shrublands (%) Trees/Shrubs/Herbs Mosaics (%) Natural/Croplands Herbaceous Mosaics (%)
Landscape Heterogeneity (year of fire ignition)	Land Cover Diversity (Shannon Index, H) Land Cover Evenness (Pielou Index, E)

498

499 All models were trained using the *ranger* R package (Wright and Ziegler, 2017) with quantile regression
 500 forests (Meinshausen, 2006). We used 500 trees, a minimum node size of 5, variance-based importance,
 501 and the Poisson split rule, with 4 variables considered at each split. Feature selection included correlation
 502 filtering ($r > 0.8$ threshold) and preliminary importance scores. Each model was trained on 75% of the
 503 data and validated on the remaining 25%. We evaluated feature contributions using SHAP (SHapley
 504 Additive exPlanations) values.

505 In addition to these primary configurations, we trained two diagnostic RF models to assess the
 506 robustness of our results. First, a “No Topography” model was built by removing elevation and slope
 507 from the predictor set while keeping all other variables and settings identical to the Full Chaco
 508 configuration. Second, an “MS Roads” model replaced the OSM-based road-density layer with the MS-
 509 based road density, again using the same sample of fire patches, hyperparameters, and training / test
 510 split as the Full Chaco RF. These sensitivity experiments were analyzed with the same SHAP-based
 511 diagnostics as the primary models and were used to evaluate whether the RF results were robust to
 512 changes in the predictor set and road-data source.

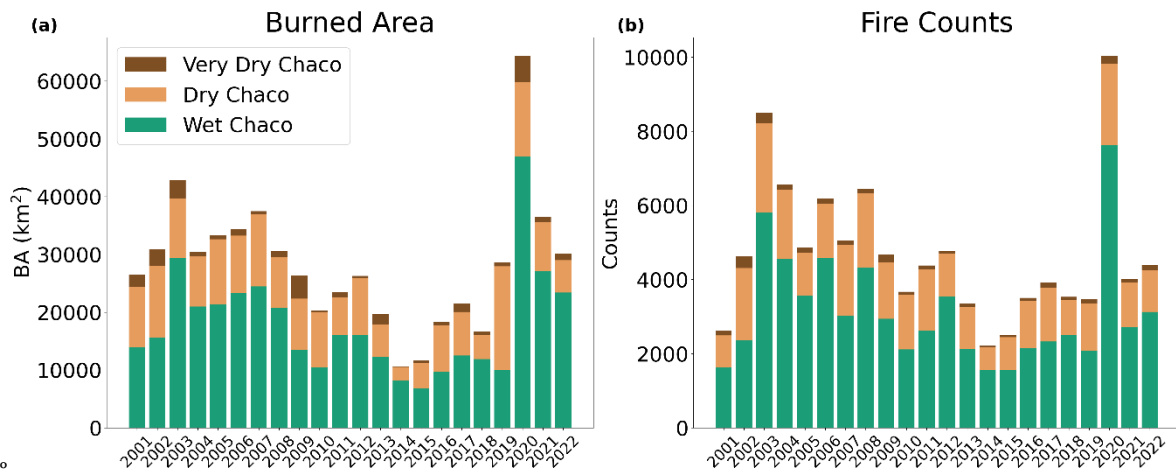
513 **3 RESULTS**

514 **3.1 Burned area and ignitions**

515 We examined the interannual variability of burned area (BA), fire counts, and mean fire duration across
516 the Gran Chaco between 2001 and 2022 (**Fig. 3; Fig. S3**). To complement these indicators, we quantified
517 the relationship between total BA and annual fire counts for each subregion and season, using linear
518 correlations (**Fig. S2**).

519 The time series reveals a sustained decrease in annual fire counts and BA from the early 2000s to the
520 late 2010s, followed by a pronounced peak in 2020–2021. Because the observational window begins in
521 2001, it is difficult to determine whether the downward phase reflects a longer-term trend or a segment
522 of decadal variability. These two peak years also show the largest BA of the record, particularly in the
523 Wet and Dry Chaco, and stand out clearly relative to the preceding trajectory.

524



525
526 **Fig. 3.** Interannual evolution of fire activity in the Gran Chaco from 2001 to 2022, derived from FRYv2.0 fire patches. (a) Total annual burned
527 area and (b) total annual fire counts, with stacked bars showing the contributions of the Wet, Dry, and Very Dry Chaco subregions.

528

529 BA and fire counts showed a broadly positive relationship, but with substantial regional and seasonal
530 differences. In the Wet Chaco, BA and fire counts were strongly correlated in both wet and dry seasons
531 ($R^2 = 0.96$ and 0.91 ; **Fig. S2**), indicating that interannual BA variability is largely explained by the
532 annual number of fire patches rather than by individual fire sizes. Mean fire duration remained stable
533 (approximately 10–12 days; **Fig. S3**).

534 The Dry Chaco exhibited a high wet-season correlation between BA and fire counts ($R^2 = 0.87$; **Fig.**
535 **S2**), but a much weaker dry-season relationship ($R^2 = 0.45$). This implies that, during the dry season,
536 fluctuations in BA are not tightly linked to fire counts, consistent with a larger contribution of size
537 extremes. Fire duration was also stable through the period (**Fig. S3**).

538 In the Very Dry Chaco, wet-season fires were infrequent and showed almost no relationship between
539 BA and fire counts ($R^2 = 0.11$; **Fig. S2**). In contrast, dry-season BA correlated strongly with the number
540 of fires ($R^2 = 0.78$). Mean fire duration was relatively constant, with no clear interannual trend (**Fig. S3**).
541 Overall, fire duration exhibited limited variation across subregions (**Fig. S3**), reinforcing that BA
542 fluctuations were controlled primarily by changes in fire counts and the distribution of fire sizes, rather
543 than by changes in the duration of individual fires.

544

545 **3.2 Land Cover and Fire size distribution**

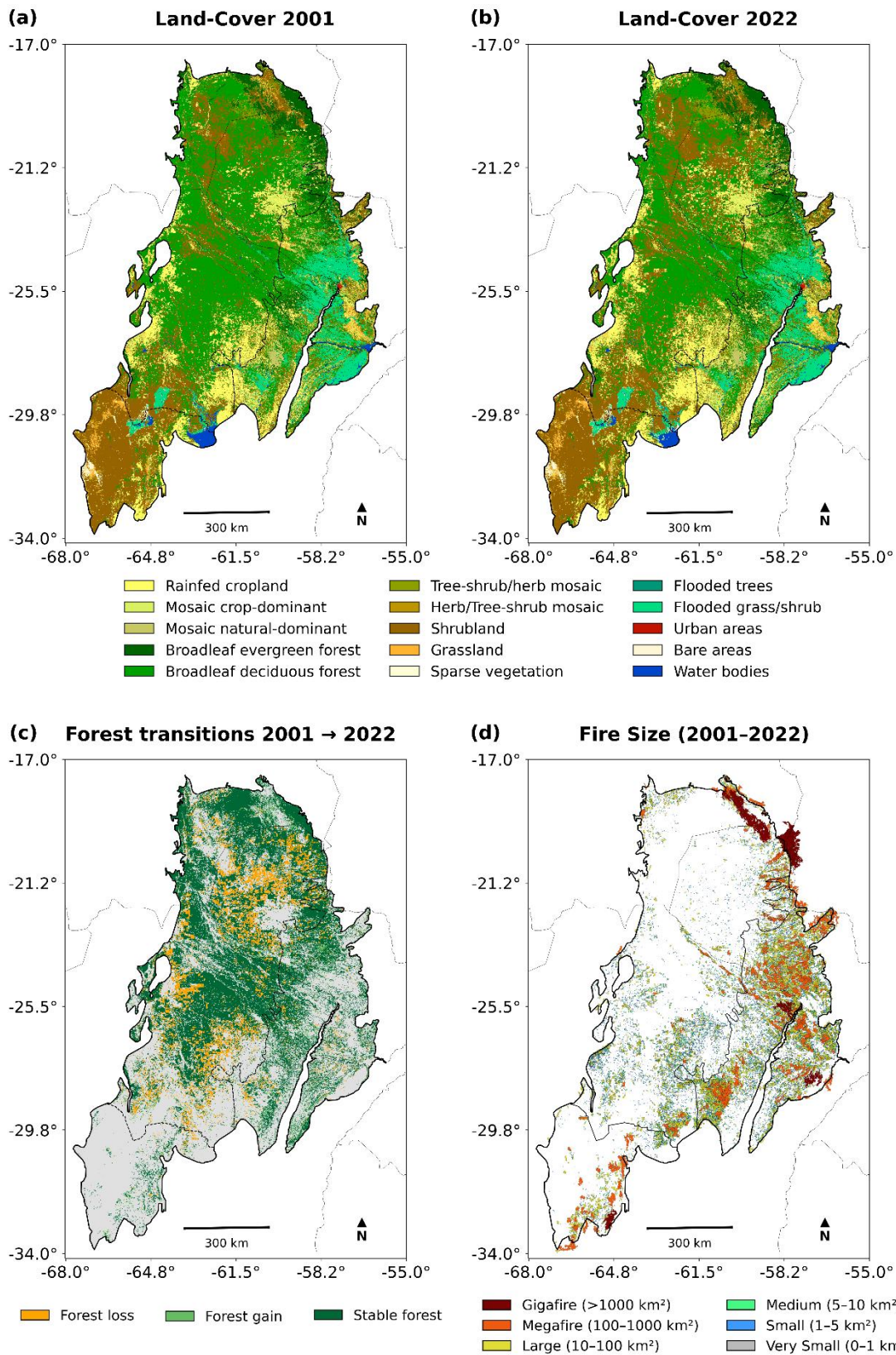
546 **Fig. 4** shows land-cover (LC) distribution in 2001 and 2022 together with the spatial distribution of fire
547 events, classified by size, between those years. Marked LC transitions occurred over the study period
548 (**Fig. 5**), with substantial expansion of shrublands and mosaic vegetation and a net reduction of tree
549 cover across the Chaco. Much of the increase in shrublands and mixed vegetation mosaics originates
550 from former tree-cover classes (**Fig. 5**), indicating widespread forest degradation and structural
551 simplification of vegetation that modifies fuel continuity.

552 Across the full Chaco, BA is dominated by open formations (**Fig. S4**): seasonally flooded grasses and
553 herbs account for ~26% of total BA, shrublands for ~23%, and mosaic vegetation for ~12%. Tree-cover
554 classes represent ~24% of total BA. Although forests are typically considered less flammable than
555 floodplain grasses and shrublands, the proportion of BA affecting tree cover is comparable to that of
556 these open formations, indicating that fires extensively affect forested and transitional landscapes.

557 Subregional patterns reinforce this contrast. In the Wet Chaco, flooded grasses and herbaceous
558 vegetation contribute more than 36% of BA, but tree cover still represents nearly one quarter,
559 showing that fire activity extends beyond floodplain systems. In the Dry Chaco, shrublands
560 dominate the burned LC composition (~39%), consistent with forest-to-shrub transitions shown
561 in Fig. 5. In the Very Dry Chaco, fires overwhelmingly affect shrublands (>75% of BA),
562 reflecting both the current dominance of this cover type and its role in sustaining large fire
563 events.

564 Fire-size distributions are strongly right-skewed in all subregions: more than 80% of events fall within
565 the Very Small (<1 km²) and Small (1–5 km²) classes (**Table S1**; **Fig. S6**). However, larger fires
566 contribute disproportionately to total BA. Megafires (100–1000 km²) are most frequent in the Wet
567 Chaco, where continuous grassland and floodplain fuel beds favor fire spread during dry periods,
568 whereas Gigafires (>1000 km²) occur predominantly across shrublands in the Dry Chaco, where fuel
569 structure and landscape openness facilitate extensive fire propagation.

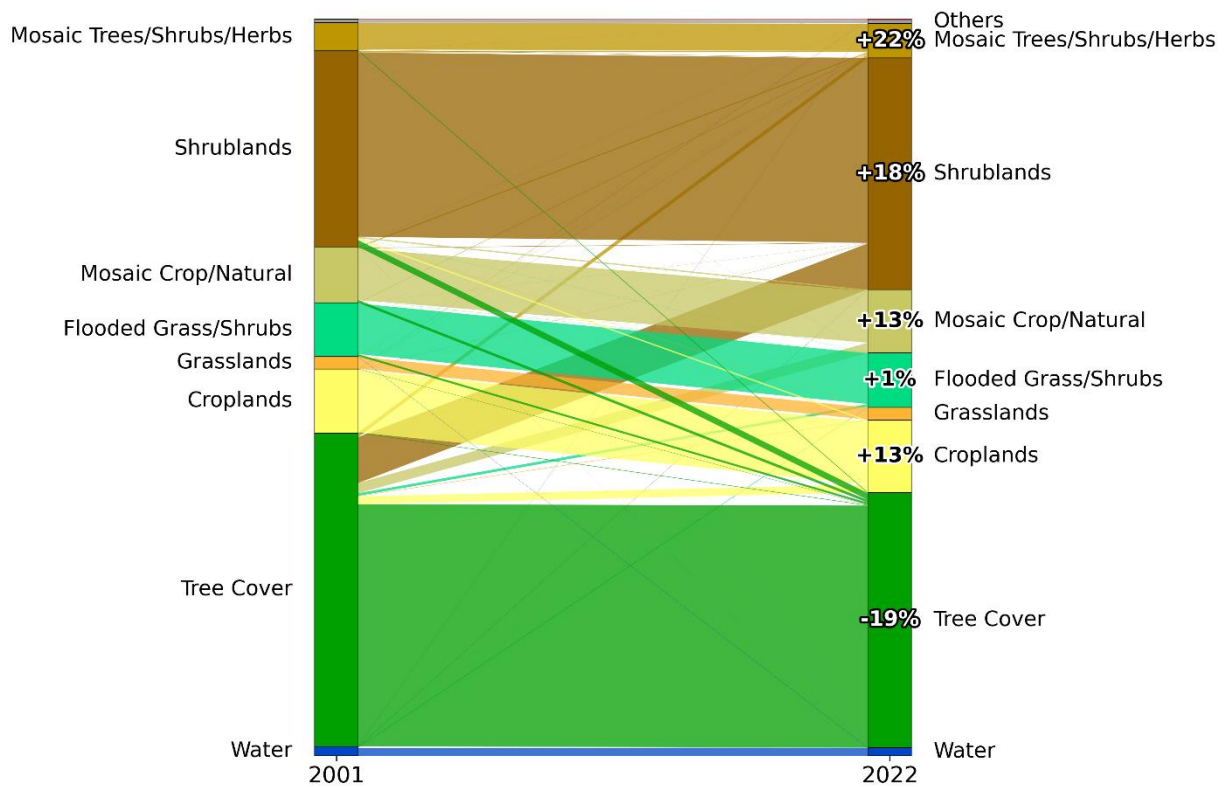
570



571
 572 **Fig. 4.** (a) and (b) Land-cover distribution in the Gran Chaco based on ESA-CCI MRLC for 2001 and 2022, respectively. (c) Forest transition
 573 classes between 2001 and 2022, showing forest loss (forest to non-forest), forest gain (non-forest to forest), and stable forest. Forests include
 574 all tree cover classes (shrubs not included); non-forest pixels appear in grey. (d) Spatial distribution of fire events (2001–2022) categorized by
 575 fire size using FRYv2.0 data. Fire-size classes range from Very Small (< 1 km²) to Gigafires (> 1000 km²). Fires patches overlapping the Chaco
 576 boundary are retained.

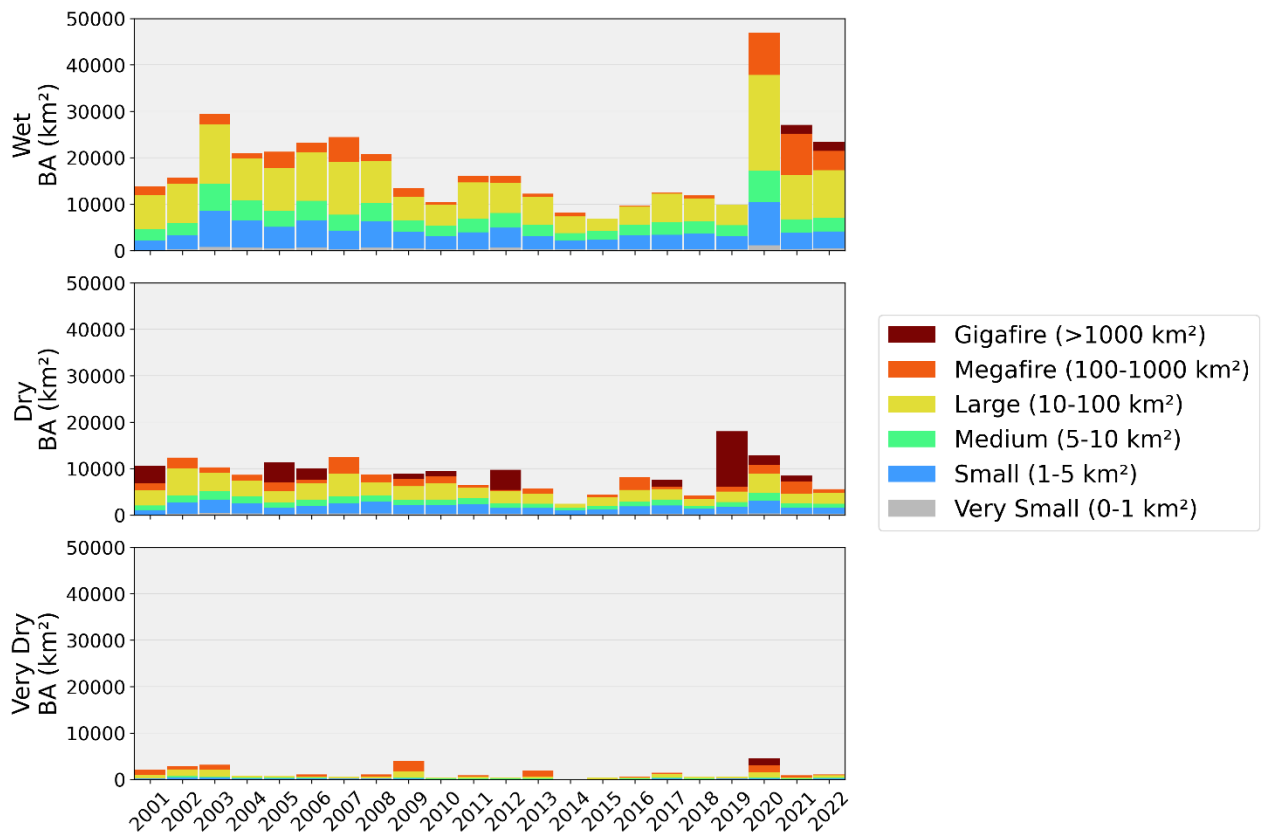
577
 578
 579
 580
 581
 582
 583
 584
 585

Forest loss is widespread across the Chaco, particularly along deforestation frontiers in Argentina and Paraguay. However, the spatial association between recent forest loss and fire size differs regionally. In Argentina, deforestation fronts frequently coincide with clusters of small and medium fires, whereas in Paraguay and Bolivia fire activity is less concentrated along recent forest-loss edges. Across all regions, most large fires occur in non-forest areas. As shown in **Fig. 5**, many of these non-forest areas correspond to former tree-cover classes converted to shrublands and mosaic vegetation, linking forest degradation to the fuel structures that sustain larger fire events.



586
 587
 588
 589
 590
 591
 592

Fig. 5. Sankey diagrams showing land-cover (LC) transitions between 2001 and 2022 across the Gran Chaco. LC classes were derived from the ESA CCI Medium Resolution Land Cover product and aggregated into the main classes present in the region. Percentages indicate the relative increase or decrease of each class between the two years. Only changes $\geq 1\%$ are shown.



593
594 **Fig. 6.** Cumulative burned area (2001–2022) by fire-size class across the Wet, Dry, and Very Dry Chaco subregions.
595

596 According to **Fig. 6**, the Wet Chaco registers the highest total burned area, nearly double that of the Dry
597 and Very Dry regions. In this subregion, large fires contribute ~40% of annual BA, and small fires ~20%
598 (**Fig. S5**). Despite their small individual extent, their high frequency (>36,000 fire events) results in a
599 substantial cumulative contribution. Extreme years such as 2003 and 2020 were marked by widespread
600 outbreaks.

601 In the Dry Chaco, fire count is lower, but large fires play a more prominent role. Large fires account for
602 about 25% of the annual BA, and gigafires can dominate totals in some years. For example, in 2019,
603 just three gigafires in the Dry Chaco burned approximately 10,000 km², equivalent to the region's mean
604 annual BA and accounting for more than half of the total that year.

605 The Very Dry Chaco, while recording the lowest overall BA, exhibits abrupt interannual peaks driven
606 by isolated megafires and gigafires, pointing to a more stochastic fire regime.

607 Between 2020 and 2022, the Wet Chaco experienced an unprecedented number of megafires and
608 gigafires, both in terms of event counts and their contribution to total BA. These patterns align with the
609 extreme fire weather anomalies described in *Section 3.3*.

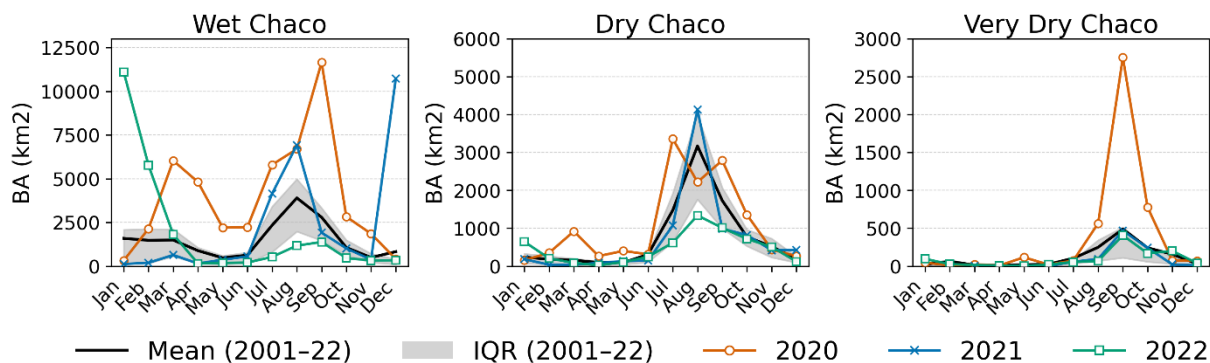
610
611

612 **3.3 Fire–weather relationship**

613

614 **Fig. 7** presents the monthly BA climatology (2001–2022) with 2020–2022 overlaid for the Wet, Dry, and Very Dry Chaco. In the Wet Chaco, BA in 2020 is above average for most months, with a secondary pulse in March–April (late wet season) preceding pronounced peaks in August–September (winter/dry season). In contrast, anomalies in 2021–2022 are concentrated in the summer/wet season (December–March), reaching levels similar to the typical late-winter/early-spring maximum, while post-winter months in 2022 remain mostly below average. In the Dry Chaco, 2020 stands out as extreme, particularly in July and September, whereas 2021 records an exceptional August at or above historical maxima and 2022 stays near or below the mean. In the Very Dry Chaco, positive anomalies are dominated by 2020, with a sharp September maximum; 2021 shows only minor increases, and 2022 remains subdued. Overall, 2020 shows widespread positive anomalies lasting several months across all subregions. In contrast, 2021 and 2022 generally feature shorter peaks, often concentrated in summer, although 2021 also records exceptional winter fires in the Dry Chaco. Activity during the canonical late-winter fire season is otherwise limited, particularly in 2022.

627



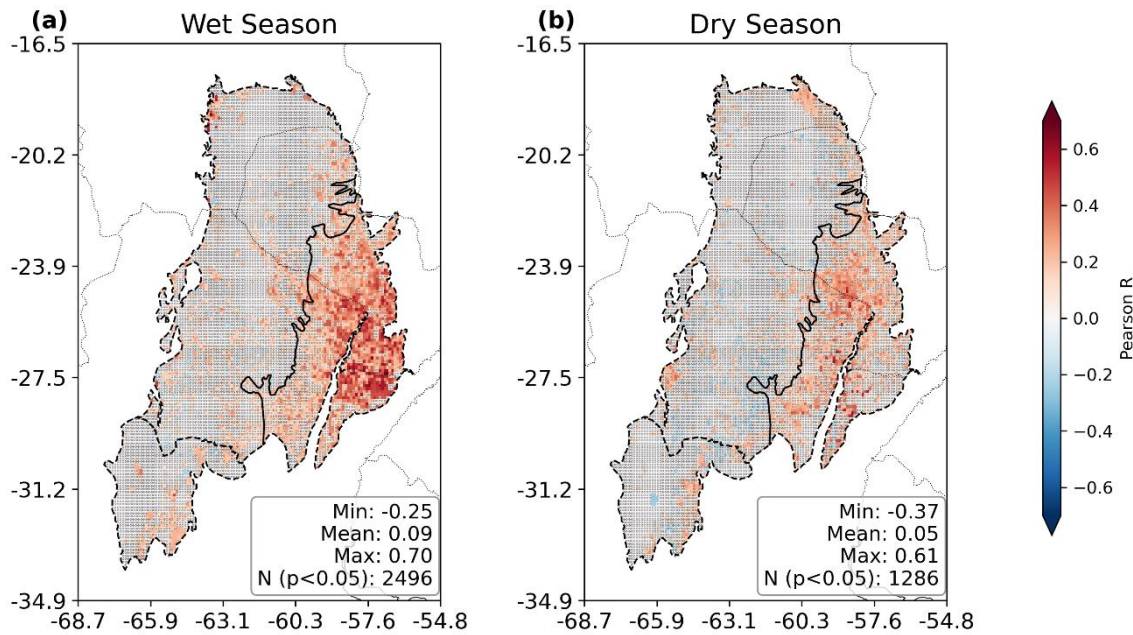
628

629 **Fig. 7.** Seasonality of burned area (BA, km²) in the Wet, Dry, and Very Dry Chaco. The black curve is the 2001–2022 monthly BA mean and the grey band shows the interquartile range (25–75%). Colored curves overlay monthly BA for 2020 (orange circles), 2021 (blue crosses), and 2022 (green squares), highlighting differences from the climatological envelope. Y-axis limits differ by panel.

632

633 The spatial patterns of fire–weather coupling shown in **Fig. 8** depict the per-pixel Pearson correlation between monthly Fire Weather Index (FWI) anomalies from ERA5-Land and BA anomalies derived from the gridded FRY dataset, both at 0.1° resolution, during the wet and dry seasons. FWI anomalies exhibit an approximately normal distribution, and after filtering pixels with fewer than four fire-active months, most BA anomaly series are quasi-normal, justifying the use of Pearson correlation as described in *Section 2.3.7*. Significant positive correlations ($p < 0.05$) are concentrated in the Wet Chaco, where R coefficients reach up to 0.7 during the wet season. In contrast, the Dry and Very Dry Chaco show weaker and more spatially scattered relationships, partly due to lower fire activity. Spearman correlations were also calculated, resulting in similar patterns with lower coefficients (maximum R of 0.52; **Fig. S7**)

642



644

645

646

647

648

649

650

651

Fig. 8. Spatial distribution of pixel-wise Pearson correlation coefficients between monthly Fire Weather Index (FWI) anomalies and monthly burned area (BA) for the period 2001–2022: (a) Wet Season and (b) Dry Season. The color bar indicates the strength and direction of the correlation (from negative in blue to positive in red). Inset statistics summarize the distribution of coefficients (Min, Mean, Max). Pixels marked with small black circles represent non-significant correlations (p -value > 0.05), while unmarked pixels indicate significant correlations (p -value < 0.05). Only pixels with more than 3-time steps with burned area > 0 were kept to avoid biased correlations related to very few or no fires.

652

653

654

655

656

657

658

659

660

661

662

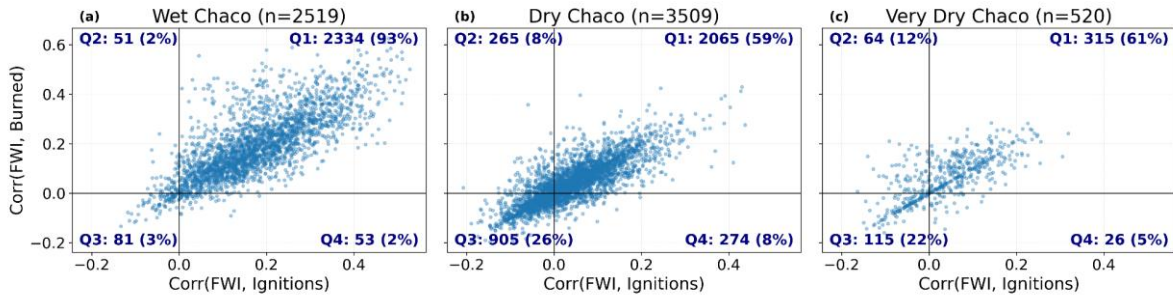
663

To further explore the spatial sensitivity of fire activity to fire weather, **Fig. 9** compares per-pixel correlations between monthly FWI anomalies (see *Section 2.3.7*) and two metrics: fire counts and BA. Each dot represents a 0.1° grid cell, and quadrants classify response types. In the Wet Chaco, 93% of cells fall in Q1, where both metrics show positive correlations with FWI, with moderate mean values (0.17 ± 0.12 for ignitions, 0.19 ± 0.13 for BA) and strong inter-metric correlation ($r = 0.76$). The Dry and Very Dry Chaco show more heterogeneous patterns, with Q1 proportions of 59% and 61%, and weaker mean correlations (~ 0.04 – 0.06). Still, inter-metric spatial correlations remain high ($r = 0.81$ and $r = 0.72$), indicating that regions more sensitive to fire weather in terms of ignitions also tend to be more sensitive in terms of fire extent.

661

662

663



664
 665 **Fig. 9.** Each panel shows a scatterplot of per-pixel Pearson correlation coefficients between the Fire Weather Index (FWI) and two fire activity
 666 metrics—ignition frequency (x-axis) and burned area (y-axis)—over the period 2001–2022. The panels correspond to the Wet, Dry, and Very
 667 Dry Chaco subregions, and each dot represents a $0.1^\circ \times 0.1^\circ$ grid cell. Quadrants are defined by the sign of each correlation coefficient to
 668 classify spatial patterns of fire–weather association: Q1 (top-right) includes pixels with positive correlations for both ignitions and burned area;
 669 Q3 (bottom-left) includes negative correlations for both; Q2 and Q4 represent divergent cases. For each subregion, quadrant counts,
 670 percentages, and summary statistics (mean \pm standard deviation of each correlation axis and Pearson r between them) are annotated.

671
 672 Finally, the temporal co-evolution of annual BA and FWI anomalies is illustrated in the appendix
 673 (**Figs. S9–S10**). Several years, especially in the Wet Chaco, show strong spatial correspondence between
 674 extensive fire activity and positive FWI anomalies (e.g. 2012, 2020–2022). However, other years (e.g.
 675 2003) reveal extensive BA without matching FWI extremes, underscoring that weather is not the sole
 676 driver of interannual variability.

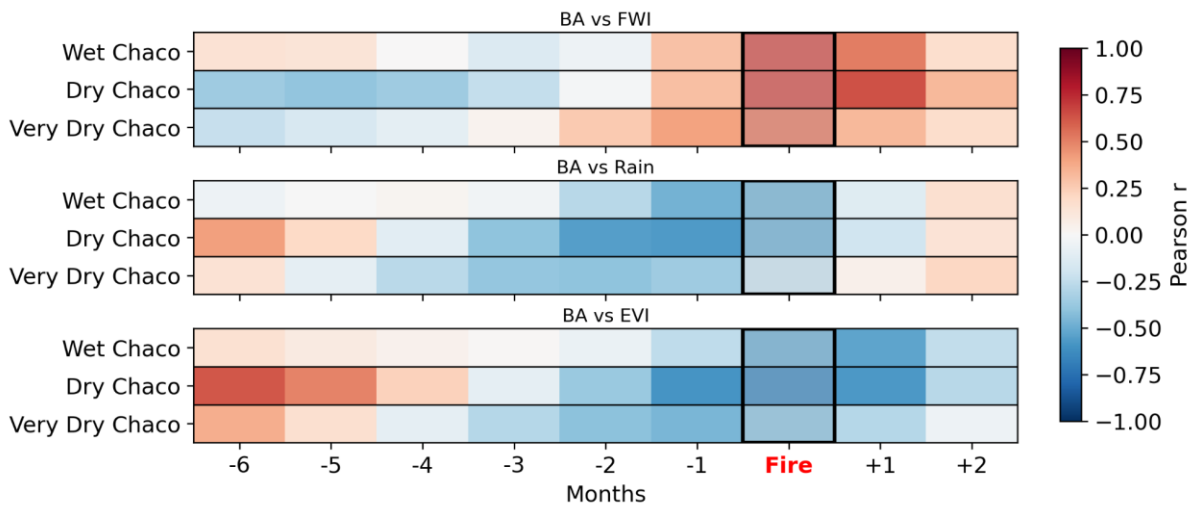
677
 678 **3.4 Temporal dynamics of fire–environment interactions**

679 To explore how conditions evolve before and after fire events, we analyzed both regional time series
 680 and lagged correlations between BA anomalies and three key drivers: FWI, rainfall, and vegetation
 681 greenness (EVI), over the period 2001–2022.

682 The time series analysis (**Fig. S10**) reveals a coherent pattern in all subregions. Typically, positive
 683 rainfall anomalies (which automatically decrease FWI) are followed by increased EVI, indicating
 684 vegetation growth and fuel accumulation. When this is then followed by elevated FWI values (due to
 685 negative rain and humidity anomalies, extreme heat and/or strong winds), peaks in BA are frequently
 686 observed. This pattern supports the interpretation of a fire-favoring sequence: moisture enables biomass
 687 build-up, which is later dried and made flammable under high fire-weather conditions, culminating in
 688 fire activity. This cycle is particularly evident in major fire years such as 2020 and 2022, especially in
 689 the Wet Chaco, where the alignment between environmental anomalies and BA peaks is striking. In the
 690 Dry and Very Dry Chaco, the sequence is also well defined, although slightly more variable probably
 691 due to limited fuel accumulation.

692 The influence of large-scale climate variability, particularly the El Niño–Southern Oscillation (ENSO),
 693 is also reflected in the fire–environment dynamics. During La Niña phases (negative ENSO), we observe
 694 reduced rainfall and elevated FWI values, often coinciding with increased BA. Conversely, El Niño

695 episodes (positive ENSO) are associated with wetter conditions, lower fire-weather pressure, and
 696 reduced fire activity (**Fig. S10** and **Fig. S11**).
 697



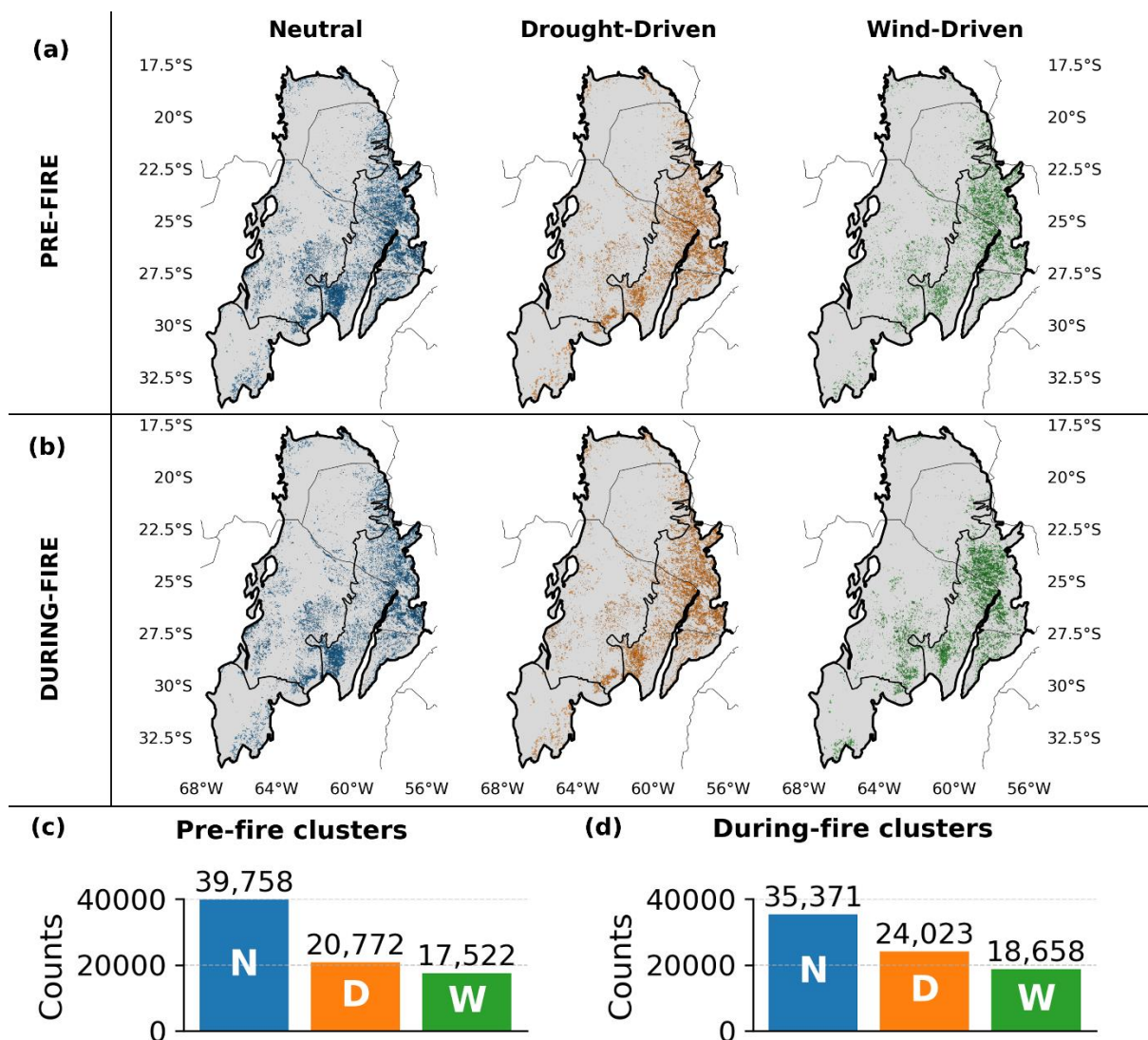
698
 699 **Fig. 10.** Lagged correlations between monthly anomalies of FWI, rainfall, and EVI with burned area in the Chaco. Each heatmap shows the
 700 Pearson correlation coefficient between the anomaly of a given variable (FWI, rainfall, or EVI) at different time lags and the burned area
 701 anomaly, for each Chaco subregion. Negative lags indicate the variable leads burned area; positive lags indicate it follows. Correlations are
 702 computed from pixel-based, region-averaged monthly time series for 2001–2022.

703
 704 **Fig. 10** shows lagged Pearson correlations between monthly anomalies of BA and FWI, rainfall, and
 705 EVI for the three Chaco subregions. Positive correlations between BA and FWI at lags 0 to +1 months,
 706 indicate that peak fire activity coincides with high fire-weather conditions. Rainfall and EVI display
 707 negative correlations with BA at short negative lags (–1 to –3 months), consistent with dry, senescent
 708 vegetation promoting flammability. At longer negative lags (–5 to –6 months), especially in the Dry and
 709 Very Dry Chaco, both variables correlate positively with BA, suggesting that wetter, greener periods
 710 months earlier promote fuel build-up. In the Wet Chaco, lag correlations are weaker and less structured,
 711 likely due to consistently moist conditions that buffer fire–environment coupling.

712
 713 **3.5 Fire-weather types**

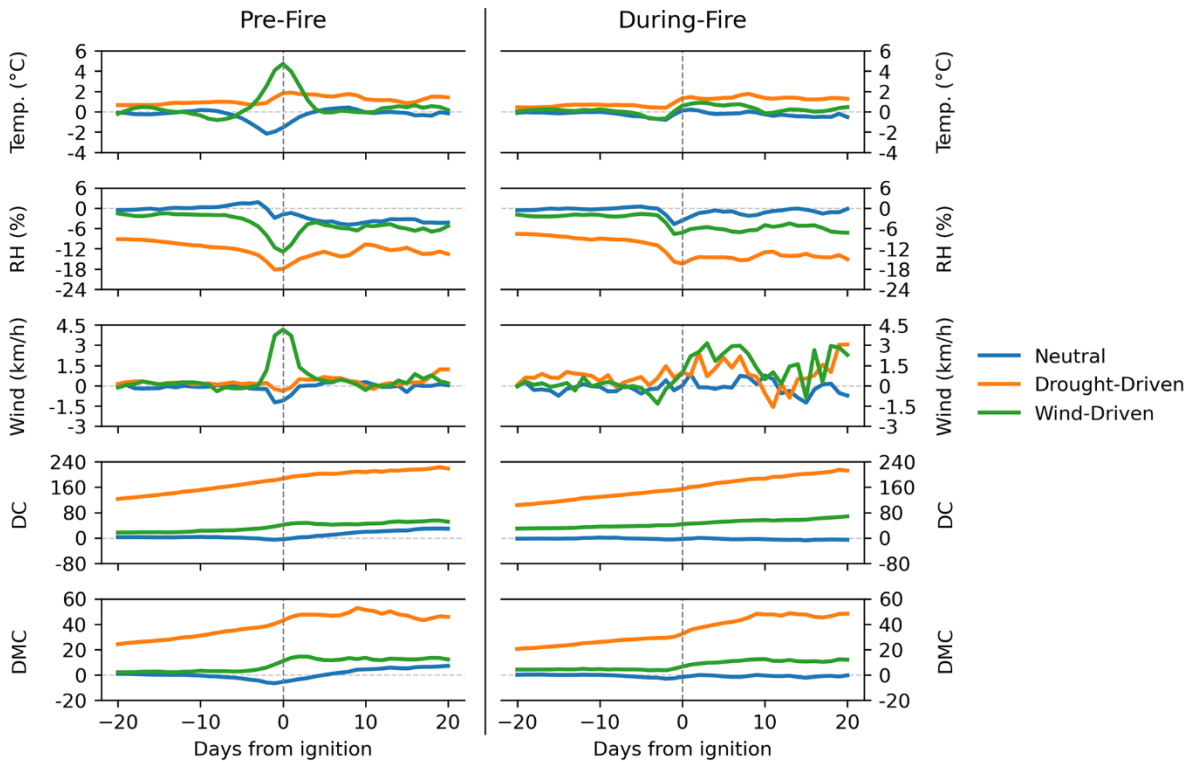
714 To characterize the atmospheric conditions associated with fire occurrence and fire growth, we analyzed
 715 the Fire–Weather Types (FWTs) assigned to each fire patch during the days preceding ignition (*Pre-*
 716 *Fire* clusters) and during the active burning period (*During-Fire* clusters). **Figure 10** presents the spatial
 717 distribution and frequency of the three FWT categories (Neutral, Drought Driven and Wind Driven) for
 718 both clustering types.

719



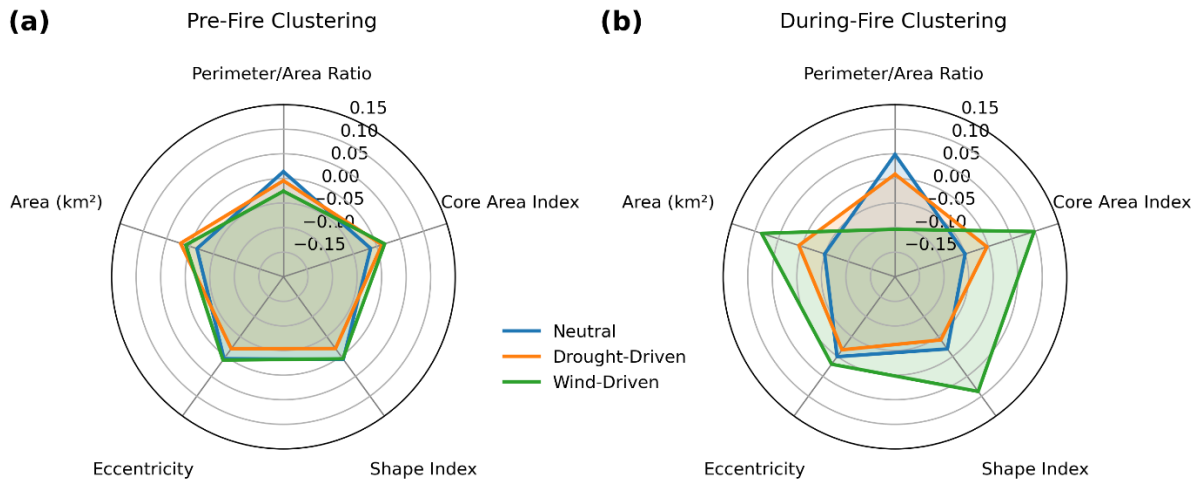
720
 721 **Fig. 11.** Spatial distribution and frequency of pre- and during-fire meteorological clusters across the Gran Chaco (2001–2022). Panels (a) and
 722 (b) show the geographic location of fire patches classified into three Fire-Weather Types (FWTs)—Neutral (blue), Drought-Driven (orange),
 723 and Wind-Driven (green)—for the pre-fire and during-fire periods, respectively, overlaid on Chaco sub-region boundaries. Some patches
 724 overlap through the years and may partially or totally cover each other. Panels (c) and (d) display the total number of patches assigned to each
 725 FWT for pre-fire and during-fire clustering methods, respectively.
 726

727 Neutral FWTs dominate both clustering groups, but their share decreases from 50.9 % to 45.3 % overall,
 728 while Drought-Driven rises from 26.6 % to 30.8 % and Wind-Driven from 22.4 % to 23.9 % (**Fig. 11c–**
 729 **d and Fig. S12**). This indicates that when fires are clustered according to the meteorology during the
 730 fire rather than before ignition, a larger fraction falls into drought or wind related conditions and fewer
 731 remain neutral. In the Wet Chaco, Neutral FWTs drop from 49 % to 42 % with a marked increase in
 732 Drought-Driven; in the Dry Chaco, both non-neutral types grow moderately; in the Very Dry Chaco,
 733 Wind-Driven types increase sharply (from 15 % to 26 %), especially in the south where complex
 734 topography may strongly influence fire-atmosphere dynamics (see *Section 2.1*). These regional shifts
 735 suggest that dryness is particularly important in the Wet Chaco, while stronger winds become
 736 comparatively more relevant in the southern Very Dry Chaco.



738
739
740
741
742

Fig. 12. Mean daily anomalies of temperature (Temp.), relative humidity (RH), 10-meter wind speed, Drought Code (DC), and Duff Moisture Code (DMC) from 20 days before to 20 days after fire ignition, averaged over fire patches assigned to the Neutral, Drought-Driven, and Wind-Driven clusters for Pre-Fire (left) and During-Fire (right) clustering approaches.



743
744
745
746
747

Fig. 13. Clusters mean morphology profiles for (a) Pre-Fire and (b) During-Fire clustering. Each axis represents a standardized morphology variable (z-score), and each colored polygon shows the mean profile for one cluster. The radial extent indicates the relative value of each variable within the dataset.

748 **Fig. 12** shows mean daily anomalies from 20 days before to 20 days after ignition for each FWT for
749 both clustering types. In the *Pre-Fire* FWT, we see that the Wind-Driven fires present a sharp rise in
750 wind speed and temperature in the days around ignition, coupled with a drop in RH, creating highly
751 flammable conditions. Drought-Driven fires exhibit a long build-up of dryness before ignition, with

752 persistently high DC and DMC values and low RH, indicating extended fuel curing. Neutral fires occur
753 under conditions close to climatology, with only small fluctuations in all variables.

754 The time series of the *During-Fire* FWTs show that the dry conditions characteristic of the Drought-
755 Driven cluster begin to develop before ignition and remain well differentiated during the fire, with very
756 low RH and high DC and DMC values. Wind speed anomalies are also elevated in this cluster, although
757 not as sharply as in the Wind-Driven cluster. This indicates that dryness and wind can co-occur in
758 Drought-Driven fires, whereas Wind-Driven fires are characterized by a clear and sustained peak in
759 wind speed combined with dry conditions, but without the prolonged build-up of drought observed in
760 the Drought-Driven cluster. The Neutral cluster remains close to climatology throughout, with only a
761 slight decrease in RH immediately prior to ignition, suggesting a minimum dryness threshold for fire
762 initiation across clusters.

763 When comparing FP morphology across clusters, *Pre-Fire* FWTs appear broadly similar (**Fig. 13, S13–**
764 **S14**), with comparable FP area, shape index (deviation from compactness), core-area index (interior
765 cohesion), eccentricity (elongation), and perimeter-to-area ratio (boundary complexity). In contrast,
766 *During-Fire* FWTs show clear differences: Wind-Driven fires tend to be larger, more elongated (higher
767 eccentricity), and more cohesive (higher core-area index and lower perimeter-to-area ratio) than
768 Drought-Driven fires, consistent with a directional spread under strong and sustained winds.

769 The combination of high eccentricity and low perimeter-to-area ratio reflects elongated but relatively
770 smooth fire perimeters produced by the rapid advancement of the fire under strong winds. In contrast,
771 Drought-Driven fires tend to generate more irregular boundaries for a given size, consistent with a
772 stronger dependence on the spatial distribution of cured fuels, which causes the fire to advance unevenly
773 across fuel patches and results in more complex and less smooth perimeter shapes.

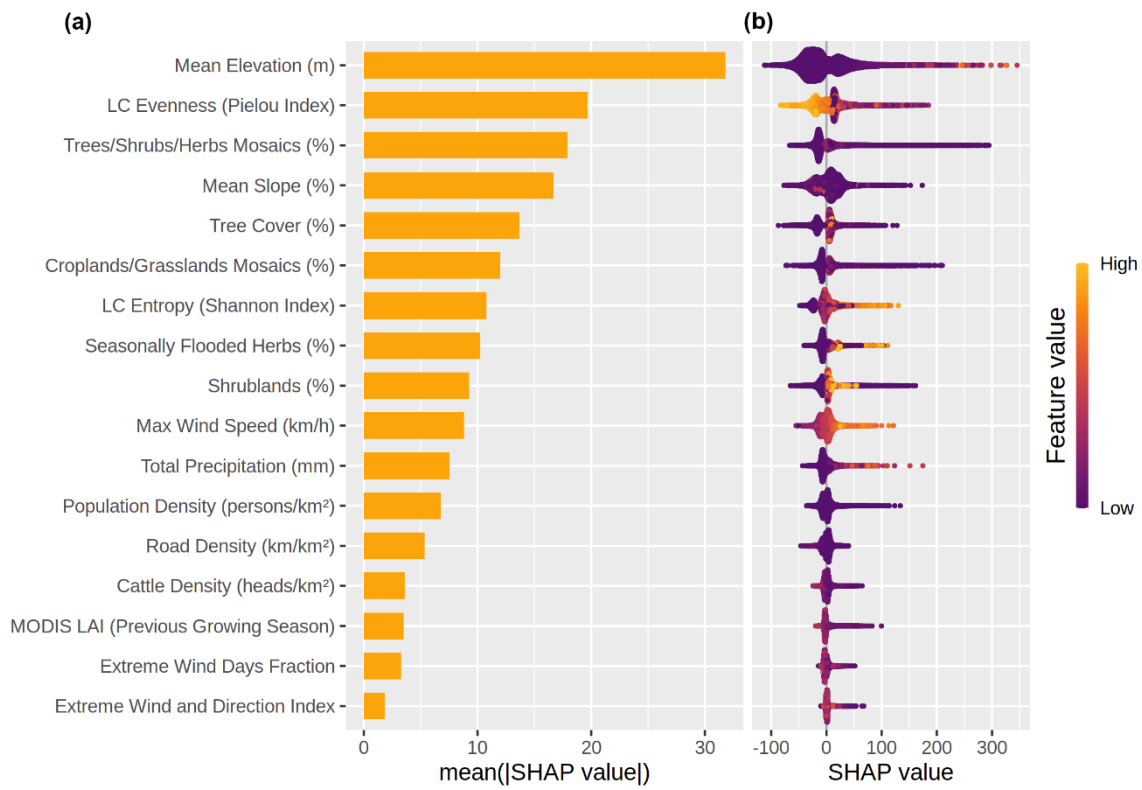
774 Overall, *Pre-Fire* FWTs capture the atmospheric conditions leading to ignition, whereas *During-Fire*
775 FWTs better reflect the conditions that shape the eventual size and geometry of the fire. These results
776 show that both clustering types capture different aspects of fire–weather interactions, but that the
777 *During-Fire* FWTs provides clearer separation in terms of final fire size and morphology.

778

779 **3.6 Fire size drivers**

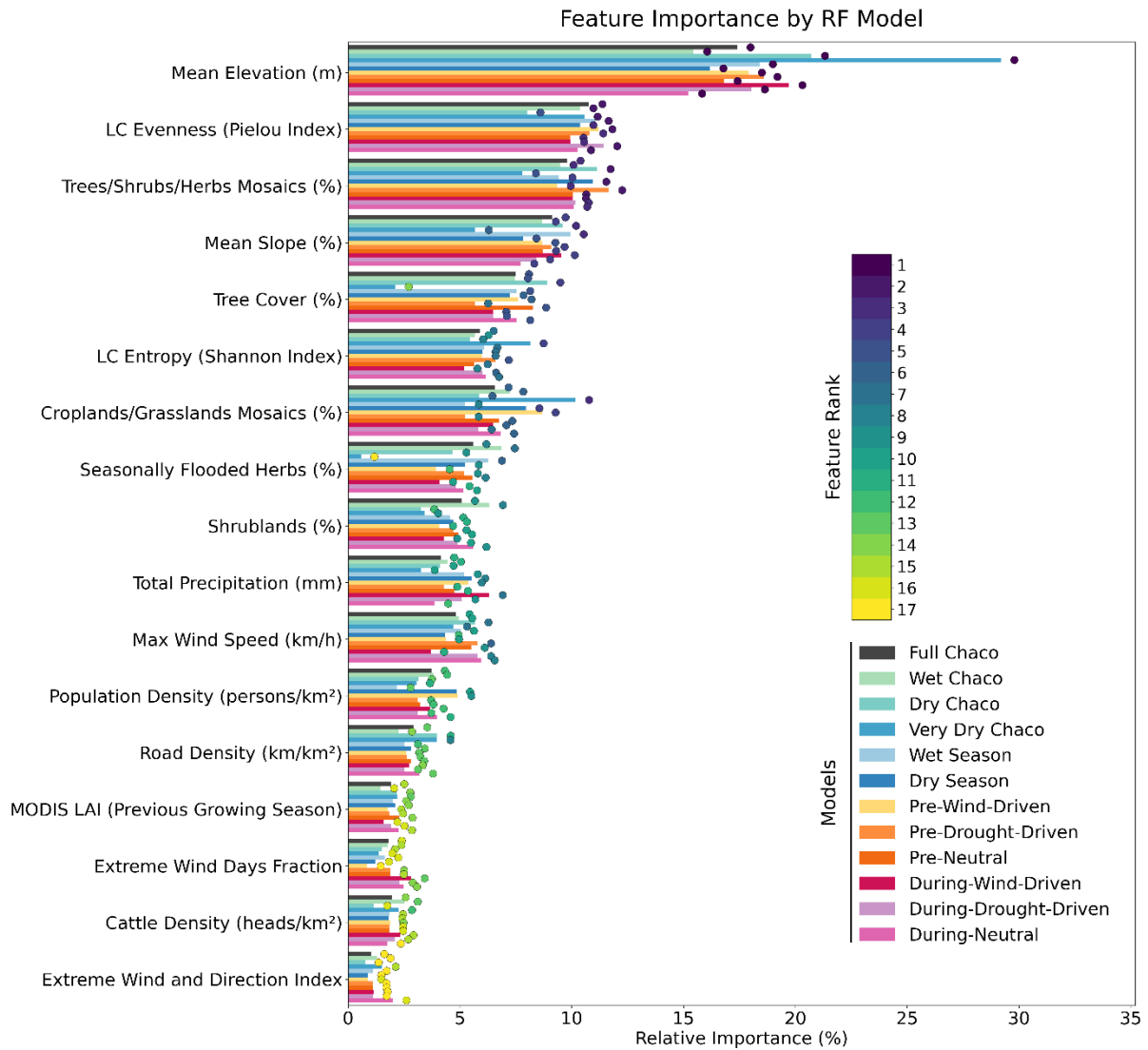
780 Our RF analysis identified static topographic and vegetation structure variables as the dominant
781 predictors of final fire size in the Gran Chaco (**Fig. 14a**). *Mean elevation* showed the highest mean
782 SHAP value (17.4%), followed by *LC evenness* (10.8%), *tree/shrub/herbs mosaics* (9.79%) and *mean*
783 *slope* (9.1%). These four variables consistently occupied the top positions across the global model and
784 all twelve specific models (**Fig. 15**). LC fractions within the FPs, including cropland or flooded
785 herbaceous cover, made moderate contributions, whereas meteorological and social variables such as
786 maximum wind speed, precipitation, population density or cattle density ranked markedly lower in

787 importance. **Fig. 15** demonstrates that this hierarchy is almost unchanged across regional, seasonal and
 788 fire-weather subsets, stable across all model configurations.
 789



790
 791 **Fig. 14.** Feature importance ranking for the Random Forest model predicting fire patch (FP) size across the entire Gran Chaco. (a) shows the
 792 average importance of each variable, expressed as the mean absolute SHAP value, which reflects how strongly each feature contributes to
 793 model predictions on average. (b) shows the SHAP values for all individual fire patches, indicating how low (purple) or high (yellow) feature
 794 values influence the prediction toward smaller or larger fires. SHAP values are used here to quantify feature importance consistently across
 795 the dataset.

796
 797 Model performance was satisfactory, with the global RF achieving a correlation of 0.74 on the test set
 798 and a test RMSE of ~110 burned pixels, compared with 0.96 and ~54 pixels on the training set (**S14**).
 799 These values indicate limited overfitting and show that the model captures a substantial fraction of the
 800 variance in fire size despite the inherent noise and strong skewness of the response variable. Because
 801 the target variable is the number of burned FRY pixels within each FP, RMSE values are interpreted
 802 directly in pixel units; with the 250 m FireCCI51 resolution, 110 pixels correspond to approximately 6.9
 803 km², less than 7 % of the 1–100 km² size range analyzed here. Comparable performance was obtained
 804 across all regional, seasonal and fire-weather configurations (**Table S3**).
 805



806

807

808

809

810

811

812

813

814

815

816

817

818

819

820

821

Fig. 15. SHAP feature importance ranks across all trained Random Forest models used to predict fire patch size (n_{cell}) based on 17 explanatory variables. Colored dots at the end of bars shows the rank of a variable’s importance (1 = most important, 17 = least important) for a given model.

Predictor distributions were often skewed (**Table S2**; **Fig. S15**), which is reflected in the SHAP spreads and dependence patterns. The global SHAP distribution (**Fig. 14b**) shows that elevation exerts a consistently positive influence on predicted fire size across most of its range, with the PDP in **Fig. 16** revealing a steep rise in SHAP values between 0 and ~40–60 m, followed by a broad plateau. Large fires dominate this low to mid elevation interval, while higher elevations generally host smaller events. This pattern reflects major physiographic contrasts in the Chaco, including low-lying floodplains and seasonal wetlands (“esteros” and “bañados”) versus slightly elevated terraces (“montes”, “albardones”) covered with woody vegetation (Bravo et al., 2025).

Regional PDPs (**Figs. S17–S19**) show the same elevation signal with different thresholds. In the Wet Chaco, SHAP values rise sharply from 0 to ~20–40 m and stabilize above that threshold, while in the Dry Chaco the increase is concentrated in the 0–20 m band and flattens near 50–100 m. In contrast, the

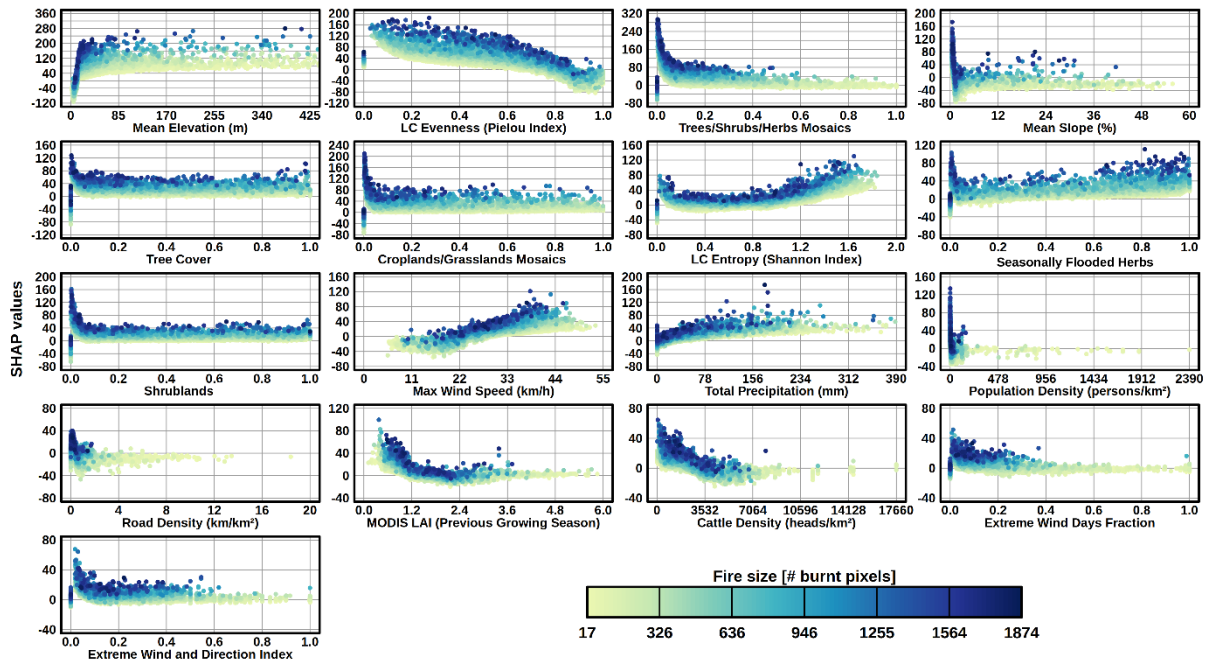
822 Very Dry Chaco exhibits a nearly linear positive gradient up to ~700 m, with large fires clearly
823 associated with higher elevation.

824 Mean slope refines this topographic signal. Although its global importance is slightly lower than
825 elevation, its SHAP dependence curve (**Fig. 16**) mirrors the elevation-driven distinction between flat
826 floodplain fuels and more fragmented uplands. SHAP values decline sharply between 0 and ~2–3 %
827 slopes, where the largest fires are concentrated, and then stabilize. In the Wet and Dry Chaco, large fires
828 are almost entirely confined to slopes below ~2–3% (**Figs. S17–S19**), whereas steeper terrain hosts only
829 small fires. The Very Dry Chaco departs from this pattern, showing a monotonic negative gradient with
830 a small cluster of large fires at intermediate slopes (~20–30 %).

831 LC evenness and LC entropy display opposite but complementary patterns as two metrics of landscape
832 heterogeneity. Evenness decreases when one or two land-cover classes dominate the patch, whereas
833 entropy increases with the number and diversity of cover types, even when their proportions are uneven.
834 Both indices are zero when only one class is present. In the global SHAP summary (**Figs. 14b and 16**),
835 many of the largest fires occur where a dominant class (low evenness) coexists with several secondary
836 LC types (intermediate entropy).

837 Across subregions, the same evenness–entropy structure emerges (**Figs. S17–S19**). Evenness shows a
838 consistently negative SHAP gradient across the Wet, Dry and Very Dry Chaco, with the transition to
839 negative contributions near 0.6 in all regions, although small and large fires occur across the full range,
840 indicating modulation rather than strict control. Entropy exhibits a more complex U-shaped structure
841 regionally, with SHAP values decreasing up to ~0.2 and rising toward intermediate entropies, where
842 large fires concentrate, before declining again at high entropy values, where only small fires are
843 observed. Overall, larger fires occur most frequently at intermediate heterogeneity levels.

844 LC fractions modulate fire size and their SHAP dependence patterns (**Figs. 14b, 16, S17–S19**) are
845 consistent with the heterogeneity indices described above. The tree–shrub–herb mosaic class shows a
846 strong and monotonic negative relationship with fire size across the entire Gran Chaco and in all three
847 regions: high fractional cover of mosaics systematically shifts SHAP values toward smaller fires,
848 whereas the largest fires appear at lower fractions of the mosaic class. Because mosaics are represented
849 as a single categorical class in CCI-MRLC, patches dominated by mosaics behave as homogeneous units
850 in the evenness and entropy indices because they count as a single LC class. Tree cover displays a
851 broadly similar negative trend in the global model and in the Wet Chaco. The regional PDPs add two
852 nuances: in the Very Dry Chaco the decline in SHAP values is nearly linear across the tree-cover
853 gradient, whereas in the Dry Chaco a secondary rise in SHAP values at high fractional tree cover
854 suggests the presence of large fires in recently deforested or thinly wooded areas still mapped as forest.
855



856
 857 **Fig. 16.** SHAP dependence plots for the 17 explanatory variables used to predict fire patch size (n_{cell}) with the Random Forest model trained
 858 on fire patches between 1 km² and 100 km² in the entire Gran Chaco between 2001 and 2022. Each panel shows the SHAP value (y-axis) across
 859 the range between 0 and the 0.995 quantile of a given feature (x-axis), illustrating the marginal effect of that feature on the model's output.
 860 Dots are colored by fire size (number of burned pixels), with darker tones indicating larger fires. Land cover classes represented as fractions.

861
 862 Shrublands exhibit contrasting SHAP responses across subregions. In the global model and in the Wet
 863 Chaco, shrub fractions show a steep negative exponential decay, with the largest fires concentrated at
 864 low shrub cover and exclusively small fires at high shrub dominance. The Dry Chaco shows the opposite
 865 pattern: SHAP values increase with shrub cover. The Very Dry Chaco exhibits a distinct, strongly non-
 866 linear shape, with SHAP values stable at low and intermediate shrub fractions but increasing sharply
 867 around ~ 0.8 - 0.9 , before declining at the extreme upper tail.

868 Flooded herbaceous vegetation shows a mixed response globally: SHAP values initially decrease
 869 between 0 and ~ 0.1 but become increasingly positive toward higher fractions, indicating that fires
 870 occurring in seasonally desiccated wetlands often reach large sizes. This flooded-herbaceous effect is
 871 concentrated in the Wet Chaco (dark points at high fractions) and is negligible in the Very Dry Chaco
 872 (large fires only where flooded cover is ~ 0 ; **Figs. S17–S19**). Cropland/grassland mosaics mirror the
 873 global shrubland pattern, with a clear negative exponential relationship in all regions: large fires almost
 874 exclusively occur at low fractions, whereas patches dominated by these mosaics generate small fires.

875 The influence of pre-fire biomass accumulation, represented by previous-season LAI, is modest in
 876 global importance but shows consistent region-specific patterns that reflect its role as a broad proxy for
 877 vegetation productivity (**Fig. 16**; **Figs. S17–S19**). At the scale of the entire Gran Chaco, SHAP values
 878 decrease strongly from low to moderate LAI, with the largest fires concentrated at LAI < 1 – 1.5 . Higher
 879 LAI values correspond to increasingly negative SHAP contributions across all regions. The regional
 880 PDPs clarify how this proxy behaves along the gradient (**Figs. S17–S19**): in the Wet Chaco, increases

881 in LAI coincide with vegetation types that tend to reduce spread regardless of their biomass; in the Very
882 Dry Chaco, the compressed LAI range reflects lower overall productivity (0-4 vs 0-6 in the other
883 regions), and large fires remain associated with the lowest values; in the Dry Chaco, a weak secondary
884 rise in SHAP values at intermediate LAI, forming a U-shape curve.

885 Meteorological predictors show consistent but secondary influences relative to topography and
886 vegetation structure (**Figs. 14b, 16, S17–S19**). Maximum wind speed exhibits the clearest signal: SHAP
887 values increase steadily with maximum wind speed up to roughly 40–45 km/h, beyond which they form
888 a plateau. In all regions, large fires cluster toward the upper half of the wind-speed distribution. In the
889 FWT-specific RF models, this effect becomes more prominent in Drought-Driven configurations, where
890 maximum wind speed attains higher SHAP-based importance ranks and larger absolute SHAP
891 amplitudes than in Neutral or Wind-Driven FWTs (**Fig. 15**).

892 In contrast, the two extreme-wind metrics (extreme wind days fraction and extreme wind-and-direction
893 index) display weak negative or near-flat SHAP responses. SHAP values decline from slightly positive
894 to near-zero between fractions of 0 and ~0.2, after which only small fires occur in all regions. The Very
895 Dry Chaco shows a shallow positive segment at very low fractions but converges toward the same
896 pattern.

897 Total precipitation shows uniformly weak contributions across regions. Although the global SHAP
898 curve appears moderately positive at low to intermediate precipitation totals, large fires are clearly
899 concentrated at low rainfall values across subregions (**Figs. S17–S19**), and small fires dominate wetter
900 intervals. The apparent positive SHAP slope at low to intermediate precipitation values reflects the
901 construction of the predictor, which integrates rainfall over the fire duration. Because longer-lasting
902 fires accumulate more rainfall within the event window, this variable is partially confounded with fire
903 duration. This structural coupling explains why some large fires appear at intermediate precipitation
904 totals despite the overall concentration of large events at low rainfall. Thus, precipitation contributes
905 only marginally to the RF predictions once static fuel and topographic structure are accounted for.

906 Human-pressure variables (road density, population density, cattle density) have consistently low mean
907 SHAP importance across all RF models (**Fig. 14a**), indicating that they explain only a minor portion of
908 the variance in fire size once topography and vegetation structure are accounted for. Nevertheless, their
909 marginal SHAP responses (**Figs. 16, S17–S19**) reveal systematic gradients that are interpretable in a
910 fire-management context.

911 Cattle density shows the clearest pattern: SHAP values decline almost monotonically with increasing
912 cattle density, and the largest fires are concentrated at low to moderate densities. At high densities,
913 SHAP values are strongly negative and large fires are absent. High stocking rates reduce standing
914 biomass and fuel continuity, limiting the capacity of fires to spread into large patches. This trend
915 is constant across all regions.

916 Road density and population density exhibit parallel patterns. SHAP values are positive at low densities
917 and become increasingly negative as infrastructure or settlement density increases. Large fires occur

918 almost exclusively where road and population density are low, whereas high-density areas are dominated
919 by small fires.

920 Despite these coherent marginal trends, the overall contribution of human-pressure variables remains
921 secondary. Their effects are largely overshadowed by static topographic structure and LC composition,
922 and their marginal signals do not alter the dominance hierarchy observed in **Fig. 15**. Overall, human-
923 pressure proxies contribute modestly once topography and vegetation structure are accounted for, and
924 they do not alter the dominant predictor hierarchy.

925

926 **3.7 Sensitivity experiments**

927 To assess the robustness of the models and the sources of explanatory power, we performed two targeted
928 sensitivity experiments: (i) training a RF without topographic variables, and (ii) replacing the baseline
929 road density product with an alternative dataset containing more detected road features.

930 In the No-Topography experiment, the overall ordering of non-topographic predictors remained stable
931 (**Fig. S20**): vegetation-structure metrics (LC evenness, mosaic cover, tree cover, LC entropy) continued
932 to dominate, while human-pressure and weather variables remained secondary. Despite this stability in
933 feature hierarchy, removing topography resulted in a marked decline in predictive performance (test
934 COR decreasing from ~0.74 to ~0.67; test RMSE increasing from ~110 to ~119 pixels; **Table S3**).
935 SHAP rankings also became less coherent, with several land-cover variables inflating artefactually in
936 importance to compensate for the absence of structural information. These changes confirm that
937 elevation and slope do not act as direct physical drivers but capture slow-varying ecological gradients
938 that distinguish floodplain herbaceous systems from slightly elevated woody landscapes, which strongly
939 condition the potential for large fire growth.

940 Although the MS road dataset detects substantially more minor linear features than OSM (see
941 Supplementary Section S4 for detailed comparison), substituting OSM with MS in the RF models
942 produced negligible changes in predictive performance and no change in feature rankings. Test COR
943 remained at 0.74 and test RMSE shifted only marginally (**Table S3**). Road density retained similarly
944 low mean SHAP importance (2–3%), and SHAP dependence curves were nearly identical across both
945 datasets. This indicates that the additional fine-scale detail captured by MS does not provide independent
946 explanatory power for final fire size at the regional scale.

947 Taken together, these results confirm three key points: (i) road density is strongly collinear with land-
948 cover composition and landscape heterogeneity; (ii) aggregating road metrics at the patch level reduces
949 sensitivity to fine-scale differences between datasets; and (iii) once other landscape variables are
950 accounted for, road density contributes only marginally to explaining final fire size at the regional scale.
951 Accordingly, substituting the road dataset does not materially affect predictive performance or feature
952 ranking. Thus, neither road dataset (OSM nor MS) provides independent explanatory power beyond that
953 already captured by topography and LC.

954 **4 DISCUSSION**

955 Building on event-level fire patches (FPs), we examine how meteorology, landscape structure, and
956 human pressures shape fire size and morphology across the Wet, Dry, and Very Dry Chaco.
957

958 **4.1 Fire regime and extreme events**

959 FP data reveal a strongly skewed size distribution: many small fires (<5 km²) and a few very large events
960 that dominate burned area (BA), consistent with global patterns (Archibald et al., 2009; Hantson et al.,
961 2015, 2017; Garca et al., 2022; Haas et al., 2022). Megafires (>100 km²) are most frequent in the Wet
962 Chaco, where continuous herbaceous fuels in savannas and seasonally flooded vegetation support
963 spread. Gigafires (>1000 km²), although rare, occur predominantly in the Dry Chaco and are often
964 concentrated in remote areas where suppression access may be limited, and where seasonally cured fuels
965 and low humidity can favor sustained spread.

966 In the Gran Chaco, most ignitions are human-caused and fire use remains widespread across rural
967 activities (Bravo et al., 2010, 2025), so the spatial and temporal distribution of fire occurrence largely
968 reflects anthropogenic pressure. However, once a fire is ignited, its final size depends more strongly on
969 fuel continuity, landscape structure and fire-weather conditions than on ignition source. Human
970 pressures and their proxies are discussed in *Section 4.5*.

971 Feron et al. (2024) show that the Gran Chaco region in South America has experienced an increase in
972 the frequency of warm, dry and flammable days, together with a rise in compound warm-dry anomalies
973 over recent decades. Although these diagnostics do not quantify fire behavior, they indicate a
974 background shift toward more frequent atmospheric conditions conducive to high flammability. In our
975 record, 2019–2022 coincides with strongly positive FWI anomalies and multiple large fire years,
976 particularly in the Wet Chaco. Despite the overall decline in BA between 2001 and the mid-2010s, the
977 clustering of extreme years at the end of the time series is consistent with increasing exposure to periods
978 of elevated fire weather under recurrent drought and large-scale climate variability (e.g. intensified La
979 Nia conditions), while noting that the satellite era remains short for robust trend detection.

980 Extreme fire periods, such as the 2019–2022 season, illustrate this sensitivity. In our record, a handful
981 of very large fires contributed a substantial share of total BA across the three subregions. This pattern
982 aligns with reconstructions of twentieth-century fire activity showing that the Gran Chaco woodlands
983 experience relatively frequent but generally low-to-moderate severity fires, with large fire seasons
984 emerging when fuel accumulation coincides with prolonged dry periods (Bravo et al., 2021, 2025; San
985 Martn et al., 2023; Vidal-Riveros et al., 2023). During 2019–2022, multi-year drought affected large
986 parts of the La Plata basin, including the Gran Chaco, reducing river discharge, soil moisture and
987 wetland extent (Naumann et al., 2023). Consistent with this hydroclimatic context, we observe
988 widespread positive BA anomalies and high FWI, particularly during 2020–2021 and especially in the
989 Wet Chaco, where rivers and floodplains typically constrain lateral spread.

990 Additionally, as discussed in the Introduction, the COVID-19 pandemic altered mobility, enforcement
991 and on-the-ground fire management across South America, with contrasted effects on fire activity
992 depending on whether restrictions reduced ignitions or weakened surveillance and suppression (Garcia
993 et al., 2021; Eklund et al., 2022; Kumar et al., 2022; Naval Fernández et al., 2023). In the Gran Chaco,
994 mobility declined during peak fire months, yet suppression capacity remained relatively stable due to
995 the continued availability of volunteer brigades, while agrarian expansion and land-clearing dynamics,
996 including deforestation burns and infrastructure projects, continued during lockdown (Castilla, 2021;
997 Naval Fernández et al., 2023; Schmidt and Castilla, 2023). Together, these observations indicate that
998 the persistence of extreme fire seasons during 2020–2022 cannot be explained solely by pandemic-
999 related changes in human activity, and that concurrent drought and elevated fire weather likely played
1000 a central role in enabling large fire spread.

1001 We therefore examined how short-term fire weather relates to BA across subregions and found strong
1002 spatial contrasts consistent with a fuel-limited to moisture-limited continuum across the Gran Chaco. In
1003 the Wet Chaco, high FWI is consistently associated with large BA, confirming moisture limitation and
1004 strong sensitivity to atmospheric conditions, in line with earlier BA-based analyses (San Martín et al.,
1005 2023) and with varying-constraint frameworks across resource gradients (Krawchuk and Moritz, 2011).
1006 In the Dry and Very Dry Chaco, correlations are weaker and more heterogeneous, indicating partial
1007 decoupling between short-term fire weather and final size, with FWI effects mediated by antecedent fuel
1008 conditions and landscape continuity, consistent with evidence that wildfire activity peaks at intermediate
1009 rainfall and productivity levels in semiarid Chaco landscapes, where fuel loads are sufficient but
1010 seasonal curing remains pronounced (Bravo et al., 2010; Argañaraz et al., 2015; San Martín et al., 2023).
1011 Lagged relationships reinforce this contrast: in drier areas, positive rainfall and vegetation productivity
1012 4–6 months before fire are followed by higher BA once fuels cure, supporting the fire–productivity
1013 hypothesis (Pausas and Bradstock, 2007) and matching wet-to-dry sequences linked to widespread burns
1014 in western and central Chaco forests (Bravo et al., 2010; Argañaraz et al., 2015; San Martín et al., 2023),
1015 whereas in wetter areas short dry spells immediately prior to fire are more predictive of activity because
1016 fuels are rarely limiting (Krawchuk and Moritz, 2011).

1017

1018 **4.2 Fire-weather types across the Chaco region**

1019 To assess how daily fire weather influences fire size, we built on the framework of Hernandez et al.
1020 (2015) and Ruffault et al. (2016, 2020), who classified Mediterranean wildfires into Fire-Weather Types
1021 (FWTs) based on pre-fire meteorological anomalies (heat, drought, wind) and found that Hot-Drought
1022 and Wind-Driven types were strongly linked to large events. Applying a similar pre-fire clustering in
1023 the Gran Chaco (Neutral, Drought-Driven, Wind-Driven) captured ignition contexts but explained little
1024 variation in final size or shape. This limited explanatory power is consistent with flat, fuel-rich systems

1025 where pre-fire anomalies modulate the probability of fire occurrence but do not reliably predict how far
1026 fires will spread once ignited.

1027 In contrast, clustering based on during-fire variables (maximum wind speed, total precipitation, drought
1028 indices, and the Extreme Wind Directionality Index developed in this study) clearly separated groups
1029 with significant differences in size and morphology. Dry, windy days during the fire, favored rapid and
1030 large expansion.

1031 Our findings contrast with Ruffault et al. (2016, 2020) and Belhadj-Kheder et al. (2020), who found pre-
1032 fire or near-ignition anomalies predictive in Mediterranean and North African settings, respectively,
1033 with the latter highlighting anomaly duration in low-suppression contexts. The stronger size–weather
1034 link for during-fire meteorology that we found likely reflects Chaco-specific traits such as a relatively
1035 flat terrain, continuous fuels, and permissive fire conditions (Bucher, 1982; Vidal-Riveros et al., 2023),
1036 which make wind and humidity more decisive than pre-fire anomalies. In the Mediterranean, fragmented
1037 fuels, complex topography, and strong suppression (Ruffault and Mouillot, 2015, 2017), translate into
1038 ignition-day extremes mattering more. A similar modulation by suppression capacity occurs in western
1039 U.S. forests (Higuera et al., 2015).

1040 In semiarid mountain landscapes of the Very Dry Chaco, Argañaraz et al. (2015) showed that climatic
1041 gradients and productivity govern where fires tend to occur, while topography and land-use mosaics
1042 constrain their spatial extent. Although their study addressed fire frequency rather than fire size, the
1043 distinction reinforces that the drivers of fire occurrence and the drivers of fire spread are related but not
1044 identical, and that landscape context mediates how daily fire weather translates into final fire extent.

1045 Our clustering extends fire-weather typologies to a tropical dry forest context and complements recent
1046 Gran Chaco regime classifications (Vidal-Riveros et al., 2024; Naval-Fernández et al., 2025) that
1047 omitted meteorological variables, highlighting the key role of fire-active weather in shaping fire
1048 morphology.

1049 These fire-weather patterns operate within a landscape where ignitions are predominantly
1050 anthropogenic, meaning that, aside from the few lightning-ignited events, human activities largely
1051 determine when and where fires start. The eventual size of these events, however, depends more strongly
1052 on daily meteorological conditions and fuel continuity, in a context where fire suppression capacity is
1053 uneven and often limited in remote areas. This contrasts with Mediterranean systems, where highly
1054 effective suppression can dampen the influence of during-fire weather on final fire size.

1055

1056 **4.3 Topography and landscape structure as primary controls of fire size**

1057 Random Forest (RF) models identified topographic, land cover (LC) and landscape-structure variables
1058 as the dominant predictors of final fire size in the Gran Chaco, with mean elevation, LC evenness, the
1059 tree–shrub–herb mosaic LC class and mean slope consistently ranking at the top of the SHAP-based
1060 hierarchy across all regional, seasonal and fire-weather configurations. The ordering remained stable in

1061 sensitivity experiments, and model performance declined when elevation and slope were removed (**Fig.**
1062 **S20, Table S3**), confirming that topography acts as an integrative proxy for geomorphological,
1063 hydrological and ecological gradients that shape the spatial context in which fires propagate. A
1064 mechanistic interpretation of vegetation effects in terms of fuel continuity and fuel moisture is developed
1065 in *Section 4.4*; this section focuses specifically on how elevation and slope structure the physical
1066 template of fire growth.

1067 Elevation captures the major physiographic contrasts that structure fuel continuity across the Gran
1068 Chaco. In the Wet Chaco, extensive low-lying floodplains and seasonal wetlands generally limit fire
1069 spread but can become highly flammable during the dry season, especially following multi-year
1070 droughts when herbaceous biomass cures over broad, continuous surfaces. The marked increase in
1071 SHAP values below approximately 20–40 m reflects these drought-prone floodplain and marsh systems,
1072 where cured grasses form highly connected fuel beds that facilitate large fire growth. In contrast, slightly
1073 elevated terraces and woody islets (“montes” or “albardones”) interrupt fuel continuity and act as natural
1074 barriers that constrain lateral fire propagation. Spatial patterns in representative Wet Chaco landscapes
1075 (**Figs. S21–S22**) support this interpretation, with large fire patches consistently associated with drought-
1076 exposed, low-elevation herbaceous systems.

1077 In the Dry Chaco, elevation contrasts distinguish floodplain matrices from agricultural mosaics and post-
1078 deforestation surfaces that break continuity. Here, the largest fires tend to occur on flat to gently elevated
1079 terrain where broad, relatively homogeneous landscape units maintain sufficiently connected fine fuels
1080 to support lateral fire growth. These tendencies align with landscape-level analyses in semi-arid central
1081 Argentina, where shrub-dominated fuel beds and topographically channeled winds promote the
1082 expansion of fire fronts (Fischer et al., 2012). In deforested landscapes, the spatial configuration of fuels
1083 is strongly shaped by clearing patterns rather than by geomorphological gradients. As a result, BA within
1084 highly fragmented agricultural or recently cleared regions (**Fig. S23**) often exhibit weaker visual
1085 correspondence with elevation contrasts, since fuel continuity arises from land-use structure rather than
1086 from topographic controls.

1087 In the Very Dry Chaco, rising elevation leads into sierran landscapes where open shrublands and xeric
1088 woodlands dominate. We found a near-linear positive association between fires and elevation up to
1089 several hundred meters, consistent with the concentration of large fires in shrub-dominated belts with
1090 continuous cured fuels along the mountains. Local examples from the Sierras de Córdoba (**Fig. S23**)
1091 demonstrate how topographic position aligns with vegetation structure. Similar relationships between
1092 physiographic position, shrub cover and extensive fire spread have been documented in other semi-arid
1093 regions of central Argentina (Fischer et al., 2012), underscoring that topography often serves as an
1094 effective proxy for the spatial organization of continuous fuels.

1095 Slope provides complementary information to elevation. The largest fires overwhelmingly occur on
1096 surfaces with slopes below approximately 2–3 %, where lateral propagation is mostly unrestricted and
1097 drainage patterns do not fragment fuels. Steeper terrain consistently hosts smaller fires across the Wet

1098 and Dry Chaco, reflecting natural fuel discontinuities. In the Very Dry Chaco, most large fires also occur
1099 at low slopes, although some events exploit elongated ridge–valley structures at intermediate slopes,
1100 particularly in the sierran environments (**Fig. S23**). The combined behavior of elevation and slope
1101 explains why removing both variables in the sensitivity experiment substantially reduced model skill
1102 (**Fig. S20**).

1103 Overall, these results indicate that topography structures the physical template within which fire growth
1104 unfolds, summarizing geomorphological and hydrological contrasts that influence where large, spatially
1105 connected burning conditions can develop. Although ignitions and land management are predominantly
1106 human-driven in the Gran Chaco, event-scale human-pressure proxies add limited incremental
1107 explanatory power once topography and landscape structure are accounted for; implications for fire use
1108 and land-use driven fuel restructuring are developed in *Section 4.5*.

1109

1110 **4.4 Vegetation structure, fuel continuity and fuel moisture**

1111 Vegetation structure exerts a central influence on fire behavior in the Gran Chaco by shaping fuel
1112 continuity and the potential for lateral spread. Across the precipitation gradient, the largest fires occur
1113 in herbaceous and shrub-dominated systems where fine fuels can become continuous and seasonally
1114 flammable, whereas woody vegetation and heterogeneous mosaics constrain propagation (San Martín
1115 et al., 2023). These patterns align with long-standing ecological characterizations of Chaco fire regimes,
1116 in which open woodlands, grass–shrub mixtures and seasonally flooded herbaceous vegetation burn
1117 more extensively and more frequently than denser forest formations (Bravo et al., 2010, 2025; Naval-
1118 Fernández et al., 2025; San Martín et al., 2023; Vidal-Riveros et al., 2023). As discussed in *Section 4.3*,
1119 these vegetation effects operate within a topographic template, but they control fire growth primarily
1120 through the composition and spatial continuity of burnable fuels.

1121 A key mechanism emerging from our results is the role of fuel continuity rather than fuel abundance per
1122 se. Herbaceous floodplain systems in the Wet Chaco and shrub-dominated systems in the Dry and Very
1123 Dry Chaco can provide highly connected fuel matrices during drought years, while woody islets, post-
1124 deforestation mosaics, cropland–grassland interfaces and other managed landscapes introduce sharp
1125 discontinuities that restrict spread. This mechanism is directly reflected in the strong importance of land
1126 cover evenness: low evenness (dominance by a single flammable class) is associated with large fires,
1127 whereas high evenness or high entropy corresponds to smaller events due to fragmentation. Similarly,
1128 the tree–shrub–herb mosaic class shows a strong negative influence, consistent with mixed woody
1129 patches acting as barriers and breaking connectivity.

1130 These structure effects are also coherent with broader evidence that increasing tree cover often reduces
1131 burned area by limiting fine-fuel continuity and increasing shade and moisture retention (Bistinas et al.,
1132 2014; Haas et al., 2022). However, exceptions are well documented where particular forest types can be
1133 more flammable than native broadleaf formations, including introduced pine plantations in some regions

1134 (Barros and Pereira, 2014; Paritsis et al., 2018; Vidal-Riveros et al., 2023). In the Chaco context, this
1135 underscores that “woody cover” is not a single fire-behavior category: the relevant control is how
1136 vegetation structure translates into horizontal continuity of ignitable fuels and seasonal drying.

1137 A second dimension is fuel moisture seasonality, which varies markedly among growth forms.
1138 Experimental and remote-sensing work in the Southern Gran Chaco indicates that shrubs and grasses
1139 reach low live fuel moisture thresholds earlier in the dry season and maintain these conditions longer
1140 than tree species (Bianchi et al., 2014; Argañaraz et al., 2016, 2018). Differences in live fuel moisture
1141 among growth forms provide a mechanistic basis for the contrasting role of shrublands along the
1142 gradient, with shrub patches often limiting spread in wetter floodplain landscapes but promoting larger
1143 fires in drier regions where shrub matrices cure rapidly and sustain combustion over large areas. This is
1144 consistent with the broader finding that shrubs and grasses can reach lower moisture contents during the
1145 dry season than tree species (Yebra et al., 2019). Flooded herbaceous vegetation likewise can function
1146 either as a barrier or as a flammable matrix depending on hydrological conditions, becoming a major
1147 driver of large burns when multi-year droughts desiccate wetlands.

1148 Productivity effects on fire behavior also emerge at broader temporal scales. We showed that vegetation
1149 greenness anomalies (EVI) respond tightly to antecedent rainfall and covary with FWI during the fire
1150 season, highlighting a classic fuel–productivity pathway: wet periods promote biomass accumulation,
1151 followed by curing during dry spells that increases flammability. This mechanism is widely documented
1152 in semi-arid Chaco systems (Bravo et al., 2010; Argañaraz et al., 2015; San Martín et al., 2023). In
1153 contrast, previous-season LAI, used here as a coarse proxy for accumulated biomass, played a
1154 comparatively minor role. LAI integrates total canopy foliage, including woody components, and
1155 therefore does not isolate the herbaceous and shrub layers most critical for fire spread. This likely
1156 explains its weak association with fire size in our models and reinforces the importance of considering
1157 fuel type and structure, rather than total leaf area, when interpreting vegetation controls on fire behavior
1158 in the Chaco.

1159 Taken together, these results show that vegetation structure mediates fire size in the Gran Chaco through
1160 three complementary mechanisms: (i) the fuel type and its degree of continuity across the landscape,
1161 which determines how far fires can propagate; (ii) the seasonal and interannual dynamics of fuel
1162 moisture, which vary among plant growth forms and strongly influence the timing and intensity of
1163 burning; and (iii) the productivity–curing sequence that links antecedent rainfall, herbaceous biomass
1164 accumulation and subsequent desiccation. These mechanisms operate differently along the
1165 precipitation–aridity gradient, producing distinct spatial fire regimes but a consistent overall pattern:
1166 large fires emerge primarily in continuous, fine-fuel systems that undergo strong seasonal drying, while
1167 fragmented or woody-dominated landscapes constrain spread regardless of weather conditions.

1168

1169 **4.5 Human pressures and fire use in the Gran Chaco**

1170 Fire regimes worldwide are tightly linked to human activity: most ignitions are anthropogenic, and both
1171 land-use change and active suppression have reshaped BA patterns in many regions (Bowman et al.,
1172 2009, 2011; Archibald et al., 2013; Andela and van der Werf, 2014; Andela et al., 2017). The Gran
1173 Chaco fits within this global picture. It is a human-dominated dry forest and savanna system where fire
1174 is at once a natural ecological process and a widespread management tool, particularly in rangelands
1175 and agricultural frontiers (Bucher, 1982; Kunst and Bravo, 2003; Bravo et al., 2010, 2025).

1176 Within the Gran Chaco, fire use is deeply embedded in pastoral and agricultural practices. Historical
1177 and ethnographic accounts document the use of fire by indigenous and rural communities in the Chaco
1178 and neighboring ecoregions for hunting, communication, warfare and the management of plant resources
1179 (Arenas, 2003; Junk and Nunes da Cunha, 2012; Sugiyama et al., 2025). As in other tropical dry regions,
1180 most events are human-ignited and intentional, associated with land clearing, slash-and-burn
1181 deforestation or the disposal of residues, with a smaller fraction being accidental or natural (Baumann
1182 et al., 2018; De Marzo et al., 2023; Gasparri and Baldi, 2013; Gürtler, 2009). Modern land users
1183 routinely burn grasslands and savannas at the end of the dry season to stimulate grass regrowth and
1184 improve forage quality, often under informal or weakly regulated conditions (Kunst and Bravo, 2003;
1185 Kunst et al., 2016; Coronel et al., 2021; San Martín et al., 2023; Bravo et al., 2025). Many fires start in
1186 managed or unmanaged grasslands, savannas or croplands and subsequently spread into neighboring
1187 forests and shrublands (Bravo et al., 2010; Tálamo et al., 2013; Loto and Bravo, 2020; Giorgis et al.,
1188 2021; De Marzo et al., 2022). In this context, exotic grasses have been shown to enhance fuel continuity
1189 and fire intensity in several dryland systems (D'Antonio and Vitousek, 1992; Kunst et al., 2016; Bravo
1190 et al., 2025), but their spatial extent and dominance within the Gran Chaco remain heterogeneous and
1191 poorly constrained at regional scales. They should therefore be regarded as one of several possible
1192 mechanisms influencing fuel structure, rather than as a pervasive or dominant driver of large fires.

1193 A further anthropogenic dimension concerns deforestation fires and the diverse forms of land-clearing
1194 burns that accompany agricultural expansion. In the Gran Chaco, the agricultural frontier has advanced
1195 rapidly over the past decades, and fire is routinely used to remove woody debris and prepare newly
1196 cleared fields, often as part of slash-and-burn cycles (Baumann et al., 2018, 2022; Boletta et al., 2006;
1197 De Marzo et al., 2023; Gasparri and Baldi, 2013; Gürtler, 2009). These fires can be extensive, but their
1198 spatial footprint depends strongly on how clearing interacts with fuel continuity, woody debris loads
1199 and local weather (San Martín et al., 2023).

1200 A similar challenge applies to prescribed and semi-prescribed burns, which are widespread in rangeland
1201 management but rarely conducted under formal prescriptions or systematic monitoring frameworks
1202 (Bravo et al., 2025; Coria et al., 2021, p.202; Kunst et al., 2016; Kunst and Bravo, 2003). Many burns
1203 are intended to be low-intensity pasture treatments undertaken in late winter or early spring, yet under
1204 drought or wind anomalies they may escape control and evolve into landscape-scale events, as

1205 documented in multiple regions of the Chaco. Although global inventories of prescribed fire exist (Hsu
1206 et al., 2025), they do not cover the Gran Chaco, underscoring the need for regional efforts to differentiate
1207 intentional, escaped and accidental fires. The lack of this information helps explain why our human-
1208 pressure variables account for little variance in final fire size: the signal of fire use is embedded within
1209 vegetation structure, fuel loads and land-cover mosaics, rather than through independent demographic
1210 metrics or ignition proxies that lack temporal and operational detail.

1211 In this context, our finding that human-pressure variables play a secondary role in predicting final fire
1212 size does not imply that humans are unimportant for the fire regime, but rather that their influence is
1213 mediated primarily through long-term land-use change and fuel restructuring. FRY v2.0 and related
1214 satellite products cannot distinguish between wildfires, escaped prescribed burns, deforestation fires or
1215 routine pasture burns, and thus the anthropogenic component enters the analysis mainly through its
1216 imprint on vegetation structure, land-cover mosaics and fuel continuity. As discussed in *Sections 4.1*
1217 *and 4.4*, the extreme fire seasons of 2019–2022 occurred during a prolonged La Niña episode that
1218 produced exceptional drought across the La Plata basin (Naumann et al., 2023; San Martín, 2024; Bravo
1219 et al., 2025). Despite changes in mobility and surveillance during the COVID-19 pandemic, large fires
1220 remained concentrated in fuel-rich, drought-stressed landscapes, indicating that climatic anomalies and
1221 fuel structure set the upper bound for fire size, while humans primarily determine ignition timing and
1222 location.

1223 Livestock production offers a clear example of how human pressures modulate fire regimes indirectly.
1224 Grazing can interrupt the positive feedback between grasses and fire by reducing fine fuels, altering
1225 vegetation composition and promoting woody encroachment (Adámoli et al., 1990; Cingolani et al.,
1226 2013; Coria et al., 2021; Bravo et al., 2025). A global analysis showed that higher livestock densities in
1227 tropical rangelands are associated with lower fire frequency and increased shrub and dwarf tree cover
1228 (Bernardi et al., 2019), and regional syntheses for the Gran Chaco report that grazing interferes with
1229 fire–grass feedbacks and contributes to shrub expansion (Alessio et al., 2008; Alinari et al., 2015; Vidal-
1230 Riveros et al., 2023). The SHAP gradients we obtained for cattle density mirror these findings: large
1231 fires are concentrated at low to moderate densities, while high-density ranching landscapes are
1232 dominated by small events, consistent with a scenario where heavy grazing reduces continuous fine
1233 fuels and increases woody cover, thereby limiting maximum fire size even if fire weather remains
1234 conducive.

1235 Road density and accessibility show a similar, albeit more complex, relationship. Numerous studies
1236 indicate that road expansion can both increase ignitions and fragment landscapes, thereby reducing the
1237 maximum size of individual fires (Andela and van der Werf, 2014; Bowring et al., 2024). In our analysis,
1238 both OpenStreetMap and Microsoft road detections density exhibited the same marginal pattern: large
1239 fires occur predominantly in areas with low road density, whereas regions with high road density are
1240 dominated by small fires. The sensitivity experiment substituting OSM with Microsoft roads confirmed
1241 that this pattern is robust and that differences in road datasets have negligible impact on predictive

1242 performance when medium to high resolution topography and LC mapping are included. The low overall
1243 importance of road density likely reflects two structural issues. First, road networks are strongly
1244 collinear with geography, LC composition and landscape heterogeneity, so much of their influence on
1245 fragmentation and suppression potential is already encoded by those variables. Second, averaging road
1246 density at the FP scale erases the spatial configuration of roads relative to ignition points and spread
1247 pathways, which is critical for understanding how roads constrain or redirect fire fronts.
1248 Population density exhibits a comparable gradient, with sparse human presence associated with larger
1249 fires and densely populated areas dominated by smaller events, consistent with more active suppression,
1250 earlier detection and greater fuel management in productive landscapes. However, remotely sensed data
1251 and coarse demographic layers cannot capture the full social dimension of fire, including local
1252 perceptions, traditional burning practices and informal suppression. Recent reviews emphasize that the
1253 perspectives and knowledge of local communities are rarely incorporated into peer-reviewed fire
1254 research in the Gran Chaco, despite being widely discussed in grey literature and the media (McDaniel
1255 et al., 2005; Devisscher et al., 2016, 2019; Coronel et al., 2021; Vidal-Riveros et al., 2023). San Martín
1256 et al. (2023) and Bravo et al. (2025) explicitly call for interdisciplinary approaches that combine
1257 environmental and social sciences to better understand human–fire interactions in this region.
1258 Overall, our results suggest that anthropogenic influences on fire size in the Gran Chaco operate mainly
1259 through their cumulative effects on vegetation structure, fuel continuity and landscape fragmentation,
1260 rather than through direct, independently measurable controls at the event scale. Ignitions are
1261 overwhelmingly human-driven, but the final size of fires is governed by the interaction between this
1262 ignition pressure, long-term land-use trajectories and the windows of opportunity created by drought
1263 and fire-conducive weather. Future work that integrates spatially explicit ignition records, fine-scale fuel
1264 management data, and socio-cultural information on fire use would allow a more complete
1265 quantification of the human contribution to fire size distributions in this rapidly changing dry forest
1266 biome. One good example of the potential of such interactions is presented in Hernández et al. (2022),
1267 who show that climate-related risks in rural Chaco communities can only be understood through
1268 frameworks that combine environmental diagnostics with local practices, knowledge systems and power
1269 relations. Their coproduction process demonstrates that the way people perceive, monitor and respond
1270 to climatic hazards fundamentally shapes exposure and outcomes. A comparable socio-environmental
1271 approach applied to fire research could reveal how decisions about land clearing, burning, suppression
1272 and access interact with drought and fuel conditions to determine whether an ignition remains small or
1273 develops into a large fire.

1274

1275 **4.6 Limitations and perspectives**

1276 Several limitations of this study stem from the nature of the available datasets and from methodological
1277 constraints. First, the meteorological information used to characterize fire weather, which relies on

1278 ERA5-Land at 0.1° resolution and cannot resolve local wind acceleration, channeled flows, shading, or
1279 fine-scale thermal gradients that influence fire spread in heterogeneous terrains. Although maximum
1280 wind speed and directional persistence emerged as meaningful predictors, the coarse resolution likely
1281 under-represents sub-kilometer variability in fire-atmosphere coupling, particularly in sierran
1282 environments. In addition, ERA5-Land precipitation is not bias-corrected, and its known tendency to
1283 smooth short-lived convective events at sub-daily scales may influence variables derived from it, such
1284 as total precipitation during the fire, potentially dampening the detection of sharp wetting or drying
1285 transitions within the time window of fire growth. Advances in downscaling techniques for wind
1286 (Dujardin and Lehning, 2022), solar radiation (Druel et al., 2025), and temperature (Kusch and Davy,
1287 2022) may improve the spatial realism of these variables in future fire regime analyses, especially in
1288 complex landscapes. However, these approaches were not applied here.

1289 Second, the FRY v2.0 dataset inherits all structural uncertainties of FireCCI51, including omission of
1290 small or low-intensity burns, overestimation in heterogeneous pixels, and potential inconsistencies in
1291 early MODIS years (Lizundia-Loiola et al., 2020; Pettinari et al., 2021). The reconstruction of FPs also
1292 depends on temporal grouping parameters that merge or split neighboring pixel clusters (Oom et al.,
1293 2016; Moreno et al., 2021). These issues constrain our ability to resolve very small events, the fine-scale
1294 geometry of scars, and rapid-fire spread fronts. The development of higher-resolution BA products has
1295 been repeatedly requested by the fire science community (Mouillot et al., 2014), and regional examples,
1296 such as the FireCCISFD20 product at 20 m for Africa (Chuvieco et al., 2022), have already demonstrated
1297 large gains in BA detection. Such advances will be essential to quantify fire size distributions and fire
1298 spread processes more accurately across the Gran Chaco.

1299 Third, the satellite BA products used here do not provide information on fire type and therefore cannot
1300 distinguish among wildfires, escaped prescribed burns, deforestation fires, and routine rangeland burns.
1301 This restricts our capacity to attribute human-driven fire dynamics directly, since the anthropogenic
1302 signal enters the models primarily through long-term structural changes in vegetation composition,
1303 fragmentation and fuel continuity rather than through explicit information on ignition sources or
1304 operational decisions. The absence of spatially explicit ignition datasets, suppression records and fine-
1305 scale fuel management layers further limits our ability to separate environmental controls from
1306 management outcomes.

1307 In the absence of direct information on fire type or ignition mechanism, human-pressure variables such
1308 as road density, population density or cattle density are used as indirect proxies for socio-environmental
1309 processes. Their weak importance in the RF models should therefore not be interpreted as evidence that
1310 human influence is negligible, but rather as a reflection of the limited thematic precision, spatial
1311 resolution and temporal representativeness of the available demographic and infrastructure datasets.
1312 These proxies capture only broad accessibility and land-use patterns, and they cannot represent
1313 operational decisions, intentional fire use or suppression capacity. As a result, landscape and LC
1314 variables at the scale of our analysis absorb much of the anthropogenic signal in our models.

1315 Fourth, additional limitations arise from the interaction between the RF framework and the structure of
1316 the predictor datasets. Tree-based ensembles and SHAP-based rankings can be sensitive to differences
1317 in data quality, spatial support and collinearity among predictors. These conditions are better met by
1318 high-quality satellite-derived predictors such as elevation and annual land-cover layers than by
1319 demographic or infrastructure datasets, which are often coarser, noisier or less spatially complete. As a
1320 result, part of the dominant SHAP importance of topography and vegetation likely reflects both genuine
1321 structural controls on fuel continuity and the statistical advantages associated with these higher-quality
1322 predictors, rather than their purely mechanistic influence. The sensitivity experiment without
1323 topography confirms that elevation and slope summarize multiple unobserved gradients, partly
1324 compensating for limitations in other predictors. Although cross-validation diagnostics suggest limited
1325 overfitting, the RF remains bound to the chosen feature set and to the aggregation scale of fire patches.
1326 Future work could evaluate machine-learning architectures that operate directly on high-resolution
1327 imagery or spatial neighborhoods, for example through convolutional or graph-based neural networks
1328 combined with richer socio-economic layers, to test whether the predictor hierarchy found here is robust.

1329 Fifth, several environmental variables used in this study should be interpreted as proxies rather than
1330 mechanistic drivers. Elevation and slope summarize hydrological, geomorphological and ecological
1331 gradients rather than exerting direct effects on combustion. Similarly, the previous-season LAI
1332 integrates productivity and vegetation structure but does not explicitly represent live fuel moisture or
1333 curing dynamics. Incorporating finer-resolution fuel moisture content datasets, daily vegetation optical
1334 depth or in situ biomass measurements (Argañaraz et al., 2016, 2018) would strengthen mechanistic
1335 interpretations.

1336 Finally, our statistical models do not capture feedbacks between fire behavior and atmospheric
1337 processes, nor do they represent dynamic suppression, diurnal cycles of wind and humidity, or sub-daily
1338 fire-growth stages. Mechanistic fire-spread models and hybrid statistical–physical approaches could
1339 help resolve these processes and offer a complementary perspective.

1340 Despite these limitations, our results provide a consistent regional picture: static landscape structure,
1341 summarized by topography and vegetation composition, dominates fire-size outcomes, while
1342 meteorology governs the windows of opportunity for rapid spread. Future work that combines high-
1343 resolution BA mapping, improved fire-weather fields, ignition and management records, and socio-
1344 cultural dimensions of fire use would allow a more comprehensive understanding of the evolving fire
1345 regime of the Gran Chaco.

1346 **5 CONCLUSIONS**

1347 This study advances understanding of fire regimes across the Wet, Dry, and Very Dry Chaco through a
1348 spatially explicit analysis of fire events from 2001–2022. We document strong regional contrasts in fire
1349 size, seasonality and morphology, and show that these patterns arise from the combined effects of fuel
1350 structure, fire weather and long-term land use change.

1351 Fire patch (FP) sizes were highly skewed: over 80% of detected fires were <5 km², yet large events
1352 dominated total burned area (BA). Megafires (>100 km²) occurred in all subregions, with the Wet Chaco
1353 recording the most. Gigafires (>1000 km²) were rare but concentrated in the Dry Chaco, where some
1354 single events exceeded 50% of annual BA. The Wet Chaco burned most extensively ($\sim 2\times$ the Dry
1355 Chaco), with the highest fire frequency and ignition density, reflecting greater biomass productivity and
1356 continuous fuels. The Very Dry Chaco, although it contributes the smallest share of total BA, is
1357 characterized by sporadic large, mega and gigafires that produce abrupt interannual peaks, consistent
1358 with a more stochastic fire regime where a few extreme events dominate variability.

1359 The Fire Weather Index (FWI) displayed its strongest and most coherent relationship with BA and fire
1360 counts in the Wet Chaco, where most pixels (93%) showed positive correlations between monthly FWI
1361 and BA anomalies (R up to 0.7), confirming a moisture limited regime. In the Dry and Very Dry Chaco,
1362 correlations were weaker and more heterogeneous, indicating that short term fire weather alone cannot
1363 explain spatial and interannual variability in BA. The extreme fire seasons of 2019–2022 coincided with
1364 a prolonged La Niña event and widespread positive FWI anomalies, especially in the Wet, yet some
1365 years with extensive burning occurred without exceptional FWI, underscoring the additional roles of
1366 fuel continuity, antecedent conditions and ignition patterns.

1367 Lagged analyses revealed a fuel productivity mechanism in drier areas and a short-term drying control
1368 in wetter ones. In the Dry and Very Dry Chaco, positive rainfall and greenness anomalies several months
1369 before the fire season were followed by higher BA once fuels cured, consistent with a productivity–
1370 curing sequence where wet periods build biomass that later dries and burns. In wetter sectors of the
1371 Chaco, shorter dry spells immediately before the fire season were more closely associated with BA
1372 peaks, reflecting conditions where fuels are rarely limiting and fire activity responds primarily to
1373 transient moisture deficits. La Niña phases strengthened fire potential across the region through reduced
1374 rainfall and elevated fire weather, and the clustering of extreme fire years at the end of the record
1375 suggests increasing exposure to such windows of opportunity.

1376 Fire weather types (FWT) provided additional insight into how daily meteorology shapes fire outcomes.
1377 Pre-fire clustering captured ignition contexts but showed limited discrimination in final size or shape,
1378 consistent with a system where ignitions are predominantly anthropogenic and occur under broadly
1379 permissive conditions. In contrast, clustering based on during-fire meteorology separated neutral,
1380 drought-driven and wind-driven fires with clear differences in size and morphology. Wind-driven events
1381 were larger, more elongated and more cohesive than drought-driven fires, highlighting fire patch

1382 morphology as a signature of strong, persistent winds that could be used to benchmark process-based
1383 fire models and emerging machine learning approaches for fire behavior prediction.

1384 Random Forest models showed that static landscape structure dominates fire size outcomes. Mean
1385 elevation, land cover evenness, a tree–shrub–herb mosaic land cover class and mean slope consistently
1386 ranked highest in SHAP based importance across regions, seasons and FWTs, ahead of meteorologic al
1387 and human pressure variables. With regional variations, large fires mostly concentrated in flat, low lying
1388 or gently elevated areas that host continuous herbaceous or shrub fuels, while steeper slopes and higher
1389 tree cover limited spread. Shrublands and flooded herbaceous vegetation played contrasted roles along
1390 the precipitation gradient, inhibiting spread in wetter, fragmented floodplains and supporting large fires
1391 in drier, shrub dominated matrices.

1392 Human pressures in the Gran Chaco are essential for ignition but emerged as secondary for explaining
1393 the variation in final fire size once landscape structure is accounted for. Cattle, road, and population
1394 density all showed interpretable SHAP gradients, with larger fires occurring in remote, sparsely
1395 populated landscapes with low accessibility and low to moderate grazing pressure, and smaller fires in
1396 heavily managed areas with high road density or high stocking levels. However, their overall importance
1397 in the models was low, reflecting that most anthropogenic effects on fire size operate indirectly through
1398 long term transformations of vegetation structure, fuel continuity and fragmentation, or that they are
1399 hard to account for through remote sensing. Deforestation and land clearing fires contributed to BA,
1400 particularly in expanding agricultural frontiers, but the largest megafires and gigafires arose when
1401 continuous fine fuels, drought and wind aligned in ways that exceeded available suppression capacity.

1402 By combining medium resolution FP data, reanalysis-based weather metrics, machine learning and
1403 landscape analysis, we identify key biophysical, climatic and anthropogenic determinants of fire size
1404 and shape in a major South American ecoregion, the Gran Chaco. Our results emphasize that topography
1405 and vegetation structure set the primary template for fire spread, that during-fire meteorology governs
1406 when ignited fires evolve into large, elongated events, and that human activities shape fire size mainly
1407 through their cumulative imprint on fuels and landscape configuration rather than through simple
1408 demographic gradients. These findings inform fire risk assessment and management under ongoing land
1409 use intensification and climate variability in the Gran Chaco, and highlight the need for high resolution
1410 BA products, improved fire weather fields, explicit ignition and management records and stronger
1411 integration of socio-cultural dimensions of fire use in order to anticipate how this fire regime will
1412 respond to future environmental and societal change.

1413

1414 **6 CODE AND DATA AVAILABILITY**

1415 The datasets used in this study are publicly available from the sources cited in Section 2.2. Fire
1416 data were obtained from the FRY/FireCCI dataset, land-cover data from the ESA Climate
1417 Change Initiative Land Cover project, and meteorological variables from ERA5-Land via the
1418 Copernicus Climate Data Store (CDS). The scripts used for data processing, statistical analysis,
1419 and figure generation were developed by the authors and are available from the corresponding
1420 author upon reasonable request.

1421

1422 **7 AUTHOR CONTRIBUTIONS**

1423 RSM collected and processed the data, analyzed the results, and drafted the manuscript. CO and AS
1424 conceived the idea and led the project. PVA contributed to data analysis, specifically by performing
1425 Random Forest modeling. All co-authors discussed the results, provided critical feedback, and reviewed
1426 the manuscript.

1427

1428 **8 COMPETING INTERESTS**

1429 The authors declare that they have no conflict of interest.

1430

1431 **9 ACKNOWLEDGEMENTS**

1432 The authors thank all the researchers and institutions involved in providing open-access datasets,
1433 including ESA CCI, ERA5-Land, and the Copernicus Climate Data Store (CDS). We acknowledge the
1434 computational infrastructure and support provided by the Laboratoire des Sciences du Climat et de
1435 l'Environnement (LSCE/IPSL). We also express our gratitude to Dr. Sandra Bravo for her important
1436 collaboration and contributions to our understanding of the fire regime in the region, as well as
1437 colleagues from CONICET for their valuable insights into Chaco ecology. The authors also
1438 acknowledge the use of AI-based tools to assist with text editing, code debugging, and figure scripting
1439 throughout the preparation of the manuscript.

1440

1441 **10 FINANCIAL SUPPORT**

1442 This research was partially funded by the European Space Agency through the Climate Change Initiative
1443 programme, under contract numbers ESA/No. 4000126564 (Land_Cover_cci) and ESA ESRIN/No.

1444 4000125259/18/I-NB. R. San Martin received doctoral funding from the Environmental Science
1445 Doctoral School of Île-de-France (DS 129). A. Sörensson acknowledges support from the Agencia
1446 Nacional de Promoción Científica y Tecnológica (ANPCyT, Argentina) via project PICT 2018-02511,
1447 and from the Consejo Nacional de Investigaciones Científicas y Técnicas (CONICET, Argentina)
1448 through grant PIP 11220200102141CO. F. Mouillot acknowledges support from the FireCCI project
1449 (<https://climate.esa.int/en/projects/fire/>, last consulted October 2023), which is part of the European
1450 Space Agency Climate Change Initiative (ESA CCI) programme (Contract No. 4000126706/19/I-NB),
1451 and from the FIRE-ADAPT project (EU grant HORIZON-MSCA-2021-SE-01086416).
1452

1453 **11 REFERENCES**

- 1454 Adámoli, J., Sennhauser, E., Acero, J. M., and Rescia, A.: Stress and Disturbance: Vegetation
 1455 Dynamics in the Dry Chaco Region of Argentina, *Journal of Biogeography*, 17, 491–500,
 1456 <https://doi.org/10.2307/2845381>, 1990.
- 1457 Alencar, A. A., Brando, P. M., Asner, G. P., and Putz, F. E.: Landscape fragmentation, severe
 1458 drought, and the new Amazon forest fire regime, *Ecological Applications*, 25, 1493–1505,
 1459 <https://doi.org/10.1890/14-1528.1>, 2015.
- 1460 Alessio, G. A., Peñuelas, J., Llusà, J., Ogaya, R., Estiarte, M., and De Lillis, M.: Influence of
 1461 water and terpenes on flammability in some dominant Mediterranean species, *Int J Wildland*
 1462 *Fire*, 17, 274–286, <https://doi.org/10.1071/WF07038>, 2008.
- 1463 Alinari, J., Muller, A. von, and Renison, D.: The contribution of fire damage to restricting high
 1464 mountain *Polylepis australis* forests to ravines: Insights from an un-replicated comparison,
 1465 *Ecología Austral*, 25, 11–18, <https://doi.org/10.25260/EA.15.25.1.0.53>, 2015.
- 1466 Andela, N. and van der Werf, G. R.: Recent trends in African fires driven by cropland expansion
 1467 and El Niño to La Niña transition, *Nature Clim Change*, 4, 791–795,
 1468 <https://doi.org/10.1038/nclimate2313>, 2014.
- 1469 Andela, N., Morton, D. C., Giglio, L., Chen, Y., van der Werf, G. R., Kasibhatla, P. S., DeFries,
 1470 R. S., Collatz, G. J., Hantson, S., Kloster, S., Bachelet, D., Forrest, M., Lasslop, G., Li, F.,
 1471 Mangeon, S., Melton, J. R., Yue, C., and Randerson, J. T.: A human-driven decline in global
 1472 burned area, *Science*, 356, 1356–1362, <https://doi.org/10.1126/science.aal4108>, 2017.
- 1473 Andela, N., Morton, D. C., Giglio, L., Paugam, R., Chen, Y., and Hantson, S.: The Global Fire
 1474 Atlas of individual fire size, duration, speed and direction, 2019.
- 1475 Archibald, S., Roy, D. P., Van WILGEN, B. W., and Scholes, R. J.: What limits fire? An
 1476 examination of drivers of burnt area in Southern Africa, *Global Change Biology*, 15, 613–630,
 1477 <https://doi.org/10.1111/j.1365-2486.2008.01754.x>, 2009.
- 1478 Archibald, S., Lehmann, C. E. R., Gómez-Dans, J. L., and Bradstock, R. A.: Defining pyromes
 1479 and global syndromes of fire regimes, *Proceedings of the National Academy of Sciences*, 110,
 1480 6442–6447, <https://doi.org/10.1073/pnas.1211466110>, 2013.
- 1481 Archibald, S., Lehmann, C. E. R., Belcher, C. M., Bond, W. J., Bradstock, R. A., Daniau, A.-
 1482 L., Dexter, K. G., Forrester, E. J., Greve, M., He, T., Higgins, S. I., Hoffmann, W. A., Lamont,
 1483 B. B., McGlenn, D. J., Moncrieff, G. R., Osborne, C. P., Pausas, J. G., Price, O., Ripley, B. S.,
 1484 Rogers, B. M., Schwilk, D. W., Simon, M. F., Turetsky, M. R., Van der Werf, G. R., and Zanne,
 1485 A. E.: Biological and geophysical feedbacks with fire in the Earth system, *Environ. Res. Lett.*,
 1486 13, 033003, <https://doi.org/10.1088/1748-9326/aa9ead>, 2018.
- 1487 Arenas, P.: ARENAS, Pastor. 2003. Etnografía y alimentación entre los toba-ñachilamole#ek
 1488 y wichí-lhuku'tas del Chaco Central (Argentina). Buenos Aires, Edición del autor, 562 p. 24x17
 1489 cm. ISBN 987-43-6483-1., Book, 2003.
- 1490 Argañaraz, Pizarro, G. G., Zak, M., Landi, M. A., and Bellis, L. M.: Human and biophysical
 1491 drivers of fires in Semiarid Chaco mountains of Central Argentina, *Science of the Total*
 1492 *Environment*, 520, 1–12, 2015.

- 1493 Argañaraz, Landi, M. A., Bravo, S. J., Gavier-Pizarro, G. I., Scavuzzo, C. M., and Bellis, L.
 1494 M.: Estimation of Live Fuel Moisture Content From MODIS Images for Fire Danger
 1495 Assessment in Southern Gran Chaco, *IEEE Journal of Selected Topics in Applied Earth
 1496 Observations and Remote Sensing*, 9, 5339–5349,
 1497 <https://doi.org/10.1109/JSTARS.2016.2575366>, 2016.
- 1498 Argañaraz, Landi, M. A., Scavuzzo, C. M., and Bellis, L. M.: Determining fuel moisture
 1499 thresholds to assess wildfire hazard: A contribution to an operational early warning system,
 1500 *PLoS ONE*, 13, e0204889, <https://doi.org/10.1371/journal.pone.0204889>, 2018.
- 1501 Arias, P. A., Rivera, J. A., Sörensson, A. A., Zachariah, M., Barnes, C., Philip, S., Kew, S.,
 1502 Vautard, R., Koren, G., Pinto, I., Vahlberg, M., Singh, R., Raju, E., Li, S., Yang, W., Vecchi,
 1503 G. A., and Otto, F. E. L.: Interplay between climate change and climate variability: the 2022
 1504 drought in Central South America, *Climatic Change*, 177, 6, [https://doi.org/10.1007/s10584-
 1505 023-03664-4](https://doi.org/10.1007/s10584-023-03664-4), 2024.
- 1506 Barros, A. M. G. and Pereira, J. M. C.: Wildfire Selectivity for Land Cover Type: Does Size
 1507 Matter?, *PLOS ONE*, 9, e84760, <https://doi.org/10.1371/journal.pone.0084760>, 2014.
- 1508 Barros, V., Clarke, R., and Silva Dias, P.: Climate Change in the La Plata Basin, Consejo
 1509 Nacional de Investigaciones Científicas y Técnicas, Buenos Aires, 2006.
- 1510 Baumann, M., Levers, C., Macchi, L., Bluhm, H., Waske, B., Gasparri, N. I., and Kuemmerle,
 1511 T.: Mapping continuous fields of tree and shrub cover across the Gran Chaco using Landsat 8
 1512 and Sentinel-1 data, *Remote Sensing of Environment*, 216, 201–211,
 1513 <https://doi.org/10.1016/j.rse.2018.06.044>, 2018.
- 1514 Baumann, M., Gasparri, I., Buchadas, A., Oeser, J., Meyfroidt, P., Levers, C., Romero-Muñoz,
 1515 A., le Polain de Waroux, Y., Müller, D., and Kuemmerle, T.: Frontier metrics for a process-
 1516 based understanding of deforestation dynamics, *Environ. Res. Lett.*, 17, 095010,
 1517 <https://doi.org/10.1088/1748-9326/ac8b9a>, 2022.
- 1518 Belhadj-Khedher, C., El-Melki, T., and Mouillot, F.: Saharan Hot and Dry Sirocco Winds Drive
 1519 Extreme Fire Events in Mediterranean Tunisia (North Africa), *Atmosphere*, 11, 590,
 1520 <https://doi.org/10.3390/atmos11060590>, 2020.
- 1521 Bernardi, R. E., Staal, A., Xu, C., Scheffer, M., and Holmgren, M.: Livestock Herbivory Shapes
 1522 Fire Regimes and Vegetation Structure Across the Global Tropics, *Ecosystems*, 22, 1457–1465,
 1523 <https://doi.org/10.1007/s10021-019-00349-x>, 2019.
- 1524 Bianchi, L., Defossé, G., Dentoni, M., Kunst, C., Ledesma, R., and Bravo, S.: Dynamics of fuel
 1525 moisture and its relation to the ecology and management of fire in the western Chaco region
 1526 (Argentina) I: basic concepts., 2014.
- 1527 Bistinas, I., Harrison, S. P., Prentice, I. C., and Pereira, J. M. C.: Causal relationships versus
 1528 emergent patterns in the global controls of fire frequency, *Biogeosciences*, 11, 5087–5101,
 1529 <https://doi.org/10.5194/bg-11-5087-2014>, 2014.
- 1530 Boletta, P. E., Ravelo, A. C., Planchuelo, A. M., and Grilli, M.: Assessing deforestation in the
 1531 Argentine Chaco, *Forest Ecology and Management*, 228, 108–114,
 1532 <https://doi.org/10.1016/j.foreco.2006.02.045>, 2006.

- 1533 Bowman, Balch, J., Artaxo, P., Bond, W. J., Cochrane, M. A., D'Antonio, C. M., DeFries, R.,
 1534 Johnston, F. H., Keeley, J. E., Krawchuk, M. A., Kull, C. A., Mack, M., Moritz, M. A., Pyne,
 1535 S., Roos, C. I., Scott, A. C., Sodhi, N. S., and Swetnam, T. W.: The human dimension of fire
 1536 regimes on Earth: The human dimension of fire regimes on Earth, *Journal of Biogeography*, 38,
 1537 2223–2236, <https://doi.org/10.1111/j.1365-2699.2011.02595.x>, 2011.
- 1538 Bowman, D. M. J. S., Balch, J. K., Artaxo, P., Bond, W. J., Carlson, J. M., Cochrane, M. A.,
 1539 D'Antonio, C. M., DeFries, R. S., Doyle, J. C., Harrison, S. P., Johnston, F. H., Keeley, J. E.,
 1540 Krawchuk, M. A., Kull, C. A., Marston, J. B., Moritz, M. A., Prentice, I. C., Roos, C. I., Scott,
 1541 A. C., Swetnam, T. W., van der Werf, G. R., and Pyne, S. J.: Fire in the Earth System, *Science*,
 1542 324, 481–484, <https://doi.org/10.1126/science.1163886>, 2009.
- 1543 Bowring, S. P. K., Li, W., Mouillot, F., Rosan, T. M., and Ciais, P.: Road fragment edges
 1544 enhance wildfire incidence and intensity, while suppressing global burned area, *Nat Commun*,
 1545 15, 9176, <https://doi.org/10.1038/s41467-024-53460-6>, 2024.
- 1546 Bravo, S., Kunst, C., Grau, R., and Aráoz, E.: Fire–rainfall relationships in Argentine Chaco
 1547 savannas, *Journal of Arid Environments*, 74, 1319–1323,
 1548 <https://doi.org/10.1016/j.jaridenv.2010.04.010>, 2010.
- 1549 Bravo, S., Kunst, C., Leiva, M., and Ledesma, R.: Response of hardwood tree regeneration to
 1550 surface fires, western Chaco region, Argentina, *Forest Ecology and Management*, 326, 36–45,
 1551 <https://doi.org/10.1016/j.foreco.2014.04.009>, 2014.
- 1552 Bravo, S., Bogino, S., Leiva, M., Lepiscopo, M., Cendoya, M., Kunst, C., and Biurrun, F.:
 1553 Wood anatomy, fire wounds and dendrochronological potential of *Prosopis pugiata* Burkart
 1554 (Fabaceae) in arid Argentine Chaco, *IAWA journal / International Association of Wood*
 1555 *Anatomists*, 42, 1–10, <https://doi.org/10.1163/22941932-bja10056>, 2021.
- 1556 Bravo, S., Ledesma, R., Coria, D., and Loto, D.: Fire in the Chaco Region: Ecological Aspects
 1557 and Land Management, in: *Fire in the South American Ecosystems*, edited by: Fidelis, A. and
 1558 Pivello, V. R., Springer Nature Switzerland, Cham, 213–241, https://doi.org/10.1007/978-3-1559-031-89372-8_8, 2025.
- 1560 Bucher, E. H.: Chaco and Caatinga — South American Arid Savannas, Woodlands and
 1561 Thickets, in: *Ecology of Tropical Savannas*, vol. 42, edited by: Huntley, B. J. and Walker, B.
 1562 H., Springer Berlin Heidelberg, Berlin, Heidelberg, 48–79, https://doi.org/10.1007/978-3-642-1563-68786-0_4, 1982.
- 1564 Bucher, E. H. and Huszar, P. C.: Sustainable management of the Gran Chaco of South America:
 1565 Ecological promise and economic constraints, *Journal of Environmental Management*, 57, 99–
 1566 108, <https://doi.org/10.1006/jema.1999.0290>, 1999.
- 1567 Cabrera, A.: Regiones fito-geográficas argentina, *Enciclopedia Argentina de Agricultura y*
 1568 *Jardinería*, 2, 1976.
- 1569 Castilla, M.: “Ahora tenemos este virus, pero cuando tenés tantos problemas en la zona nada
 1570 alcanza”: Extractivismo, segregación y pandemia en la provincia del Chaco, 2021.
- 1571 Center For International Earth Science Information Network-CIESIN-Columbia University:
 1572 Gridded Population of the World, Version 4 (GPWv4): Population Density, Revision 11,
 1573 <https://doi.org/10.7927/H49C6VHW>, 2017.

- 1574 Chuvieco, E., Aguado, I., Salas, J., García, M., Yebra, M., and Oliva, P.: Satellite Remote
1575 Sensing Contributions to Wildland Fire Science and Management, *Curr Forestry Rep*, 6, 81–
1576 96, <https://doi.org/10.1007/s40725-020-00116-5>, 2020.
- 1577 Chuvieco, E., Roteta, E., Sali, M., Stroppiana, D., Boettcher, M., Kirches, G., Storm, T.,
1578 Khairoun, A., Pettinari, M. L., Franquesa, M., and Albergel, C.: Building a small fire database
1579 for Sub-Saharan Africa from Sentinel-2 high-resolution images, *Science of The Total*
1580 *Environment*, 845, 157139, <https://doi.org/10.1016/j.scitotenv.2022.157139>, 2022.
- 1581 Cingolani, A. M., Vaieretti, M. V., Giorgis, M. A., La Torre, N., Whitworth-Hulse, J. I., and
1582 Renison, D.: Can livestock and fires convert the sub-tropical mountain rangelands of central
1583 Argentina into a rocky desert?, *Rangel J*, 35, 285–297, <https://doi.org/10.1071/RJ12095>, 2013.
- 1584 Coria, R. D., Kunst, C. R., and Bravo, S. J.: A contribution to the understanding of the woody
1585 encroachment in grasslands/savannas from the South American Semiarid Chaco., 2021.
- 1586 Coronel, G., Pastén, M., Breuer, N., Celeste, A., Rejalaga, L., Domecq, F. M., and Nagy, G. J.:
1587 Wildfires in Paraguay: Environmental and Human Impacts, in: *Sustainability in Natural*
1588 *Resources Management and Land Planning*, edited by: Leal Filho, W., Azeiteiro, U. M., and
1589 Setti, A. F. F., Springer International Publishing, Cham, 429–444, [https://doi.org/10.1007/978-](https://doi.org/10.1007/978-3-030-76624-5_25)
1590 [3-030-76624-5_25](https://doi.org/10.1007/978-3-030-76624-5_25), 2021.
- 1591 D’Antonio, C. M. and Vitousek, P. M.: Biological Invasions by Exotic Grasses, the Grass/Fire
1592 Cycle, and Global Change, *Annual Review of Ecology and Systematics*, 23, 63–87, 1992.
- 1593 De Marzo, T., Pflugmacher, D., Baumann, M., Lambin, E. F., Gasparri, I., and Kuemmerle, T.:
1594 Characterizing forest disturbances across the Argentine Dry Chaco based on Landsat time
1595 series, *International Journal of Applied Earth Observation and Geoinformation*, 98, 102310,
1596 <https://doi.org/10.1016/j.jag.2021.102310>, 2021.
- 1597 De Marzo, T., Gasparri, N. I., Lambin, E. F., and Kuemmerle, T.: Agents of Forest Disturbance
1598 in the Argentine Dry Chaco, *Remote Sensing*, 14, 1758, <https://doi.org/10.3390/rs14071758>,
1599 2022.
- 1600 De Marzo, T., Pratzler, M., Baumann, M., Gasparri, N. I., Pötzschner, F., and Kuemmerle, T.:
1601 Linking disturbance history to current forest structure to assess the impact of disturbances in
1602 tropical dry forests, *Forest Ecology and Management*, 539, 120989,
1603 <https://doi.org/10.1016/j.foreco.2023.120989>, 2023.
- 1604 Defourny, P., Lamarche, C., Brockmann, C., Boettcher, M., Bontemps, S., Maet, T., Duveiller,
1605 G. L. H., K., H. A., Kirches, G., Moreau, I., Peylin, P., Ottlé, C., J., R., Bogaert, E., Ramoino,
1606 F., Albergel, C., and Arino, O.: Observed annual global land-use change from 1992 to 2020
1607 three times more dynamic than reported by inventory-based statistics, in preparation, 2023.
- 1608 Devisscher, T., Boyd, E., and Malhi, Y.: Anticipating future risk in social-ecological systems
1609 using fuzzy cognitive mapping: the case of wildfire in the Chiquitania, Bolivia, *Ecology and*
1610 *Society*, 21, <https://doi.org/10.5751/ES-08599-210418>, 2016.
- 1611 Devisscher, T., Malhi, Y., and Boyd, E.: Deliberation for wildfire risk management: Addressing
1612 conflicting views in the Chiquitania, Bolivia, *The Geographical Journal*, 185, 38–54,
1613 <https://doi.org/10.1111/geoj.12261>, 2019.

- 1614 Doblas-Reyes, F. J., Sorensson, A. A., Almazroui, M., Dosio, A., Gutowski, W. J., Haarsma,
1615 R., Hamdi, R., Hewitson, B., Kwon, W.-T., Lamptey, B. L., Maraun, D., Stephenson, T. S.,
1616 Takayabu, I., Terray, L., Turner, A., and Zuo, Z.: Linking global to regional climate change,
1617 edited by: Masson-Delmotte, V., Zhai, P., Pirani, A., Connors, S. L., Pean, C., Berger, S., Caud,
1618 N., Chen, Y., Goldfarb, L., Gomis, M. I., Huang, M., Leitzell, K., Lonnoy, E., Matthews, J. B.
1619 R., Maycock, T. K., Waterfield, T., Yelekci, O., Yu, R., and Zhou, B., Cambridge University
1620 Press, 2021.
- 1621 Druel, A., Ruffault, J., Davi, H., Chanzy, A., Marloie, O., De Cáceres, M., Olioso, A., Mouillot,
1622 F., François, C., Soudani, K., and Martin-StPaul, N. K.: Enhancing environmental models with
1623 a new downscaling method for global radiation in complex terrain, *Biogeosciences*, 22, 1–18,
1624 <https://doi.org/10.5194/bg-22-1-2025>, 2025.
- 1625 Dujardin, J. and Lehning, M.: Wind-Topo: Downscaling near-surface wind fields to high-
1626 resolution topography in highly complex terrain with deep learning, *Quarterly Journal of the*
1627 *Royal Meteorological Society*, 148, 1368–1388, <https://doi.org/10.1002/qj.4265>, 2022.
- 1628 Eklund, J., Jones, J. P. G., Räsänen, M., Geldmann, J., Jokinen, A.-P., Pellegrini, A., Rakotobe,
1629 D., Rakotonarivo, O. S., Toivonen, T., and Balmford, A.: Elevated fires during COVID-19
1630 lockdown and the vulnerability of protected areas, *Nat Sustain*, 5, 603–609,
1631 <https://doi.org/10.1038/s41893-022-00884-x>, 2022.
- 1632 Feron, S., Cordero, R. R., Damiani, A., MacDonell, S., Pizarro, J., Goubanova, K., Valenzuela,
1633 R., Wang, C., Rester, L., and Beaulieu, A.: South America is becoming warmer, drier, and more
1634 flammable, *Communications Earth & Environment*, 5, [https://doi.org/10.1038/s43247-024-](https://doi.org/10.1038/s43247-024-01654-7)
1635 [01654-7](https://doi.org/10.1038/s43247-024-01654-7), 2024.
- 1636 Fischer, M. A., Di Bella, C. M., and Jobbágy, E. G.: Fire patterns in central semiarid Argentina,
1637 *Journal of Arid Environments*, 78, 161–168, <https://doi.org/10.1016/j.jaridenv.2011.11.009>,
1638 2012.
- 1639 Garcia, L. C., Szabo, J. K., de Oliveira Roque, F., de Matos Martins Pereira, A., Nunes da
1640 Cunha, C., Damasceno-Júnior, G. A., Morato, R. G., Tomas, W. M., Libonati, R., and Ribeiro,
1641 D. B.: Record-breaking wildfires in the world’s largest continuous tropical wetland: Integrative
1642 fire management is urgently needed for both biodiversity and humans, *Journal of*
1643 *Environmental Management*, 293, 112870, <https://doi.org/10.1016/j.jenvman.2021.112870>,
1644 2021.
- 1645 García, M., Pettinari, M. L., Chuvieco, E., Salas, J., Mouillot, F., Chen, W., and Aguado, I.:
1646 Characterizing Global Fire Regimes from Satellite-Derived Products, *Forests*, 13, 699,
1647 <https://doi.org/10.3390/f13050699>, 2022.
- 1648 Gasparri, N. I. and Baldi, G.: Regional patterns and controls of biomass in semiarid woodlands:
1649 lessons from the Northern Argentina Dry Chaco, *Reg Environ Change*, 13, 1131–1144,
1650 <https://doi.org/10.1007/s10113-013-0422-x>, 2013.
- 1651 Gasparri, N. I., Grau, H. R., and Manghi, E.: Carbon Pools and Emissions from Deforestation
1652 in Extra-Tropical Forests of Northern Argentina Between 1900 and 2005, *Ecosystems*, 11,
1653 1247–1261, <https://doi.org/10.1007/s10021-008-9190-8>, 2008.
- 1654 Ginzburg, R., Adámoli, J., Herrera, P., and Torrella, S.: Los Humedales del Chaco:
1655 clasificación, inventario y mapeo a escala regional, *Miscelánea*, 14, 121–138, 2005.

- 1656 Giorgis, M. A., Zeballos, S. R., Carbone, L., Zimmermann, H., von Wehrden, H., Aguilar, R.,
 1657 Ferreras, A. E., Tecco, P. A., Kowaljow, E., Barri, F., Gurvich, D. E., Villagra, P., and
 1658 Jaureguiberry, P.: A review of fire effects across South American ecosystems: the role of
 1659 climate and time since fire, *fire ecol*, 17, 11, <https://doi.org/10.1186/s42408-021-00100-9>,
 1660 2021.
- 1661 Gürtler, R. E.: Sustainability of vector control strategies in the Gran Chaco Region: current
 1662 challenges and possible approaches, *Memórias do Instituto Oswaldo Cruz*, 104, 52–59, 2009.
- 1663 Haas, O., Prentice, I. C., and Harrison, S. P.: Global environmental controls on wildfire burnt
 1664 area, size, and intensity, *Environ. Res. Lett.*, 17, 065004, [https://doi.org/10.1088/1748-](https://doi.org/10.1088/1748-9326/ac6a69)
 1665 9326/ac6a69, 2022.
- 1666 Hantson, S., Pueyo, S., and Chuvieco, E.: Global fire size distribution is driven by human
 1667 impact and climate, *Global Ecology and Biogeography*, 24, 77–86,
 1668 <https://doi.org/10.1111/geb.12246>, 2015.
- 1669 Hantson, S., Scheffer, M., Pueyo, S., Xu, C., Lasslop, G., Nes, E. H., and Mendelsohn, J.: Rare,
 1670 Intense, Big fires dominate the global tropics under drier conditions, *Scientific reports*, 7, 1–5,
 1671 2017.
- 1672 Harper, K. L., Lamarche, C., Hartley, A., Peylin, P., Ottlé, C., Bastrikov, V., San Martín, R.,
 1673 Bohnenstengel, S. I., Kirches, G., Boettcher, M., Shevchuk, R., Brockmann, C., and Defourny,
 1674 P.: A 29-year time series of annual 300 m resolution plant-functional-type maps for climate
 1675 models, *Earth Syst. Sci. Data*, 15, 1465–1499, <https://doi.org/10.5194/essd-15-1465-2023>,
 1676 2023.
- 1677 Hernandez, C., Drobinski, P., and Turquety, S.: How much does weather control fire size and
 1678 intensity in the Mediterranean region?, *Annales Geophysicae*, 33, 931–939,
 1679 <https://doi.org/10.5194/angeo-33-931-2015>, 2015.
- 1680 Hernández, V., Florencia Fossa Riglos, M., and Vera, C.: Addressing climate services in
 1681 SouthAmerican Chaco region through a knowledge coproduction process, *Global*
 1682 *Environmental Change*, 72, 102443, <https://doi.org/10.1016/j.gloenvcha.2021.102443>, 2022.
- 1683 Higuera, P. E., Abatzoglou, J. T., Littell, J. S., and Morgan, P.: The Changing Strength and
 1684 Nature of Fire-Climate Relationships in the Northern Rocky Mountains, U.S.A., 1902–2008,
 1685 *PLOS ONE*, 10, e0127563, <https://doi.org/10.1371/journal.pone.0127563>, 2015.
- 1686 Horn, B. K. P.: Hill shading and the reflectance map, *Proceedings of the IEEE*, 69, 14–47,
 1687 <https://doi.org/10.1109/PROC.1981.11918>, 1981.
- 1688 Hsu, A., Jones, M. W., Thurgood, J. R., Smith, A. J. P., Carmenta, R., Abatzoglou, J. T.,
 1689 Anderson, L. O., Clarke, H., Doerr, S. H., Fernandes, P. M., Kolden, C. A., Santín, C., Strydom,
 1690 T., Le Quééré, C., Ascoli, D., Castellnou, M., Goldammer, J. G., Guiomar, N. R. G. N.,
 1691 Kukavskaya, E. A., Rigolot, E., Tanpipat, V., Varner, M., Yamashita, Y., Baard, J., Barreto, R.,
 1692 Becerra, J., Brunn, E., Bergius, N., Carlsson, J., Cheney, C., Druce, D., Elliot, A., Evans, J., De
 1693 Moraes Falleiro, R., Prat-Guitart, N., Hiers, J. K., Kaiser, J. W., Macher, L., Morris, D., Park,
 1694 J., Robles, C., Román-Cuesta, R. M., Rücker, G., Senra, F., Steil, L., Valverde, J. A. L., and
 1695 Zerr, E.: A global assemblage of regional prescribed burn records — GlobalRx, *Sci Data*, 12,
 1696 1083, <https://doi.org/10.1038/s41597-025-04941-w>, 2025.

- 1697 Jones, Abatzoglou, J. T., Veraverbeke, S., Andela, N., Lasslop, G., and Forkel, M.: Global and
1698 regional trends and drivers of fire under climate change, *Reviews of Geophysics*, 60, 2020
1699 000726, <https://doi.org/10.1029/2020RG000726>, 2022.
- 1700 Junk, W. J. and Nunes da Cunha, C.: Pasture clearing from invasive woody plants in the
1701 Pantanal: a tool for sustainable management or environmental destruction?, *Wetlands Ecol*
1702 *Manage*, 20, 111–122, <https://doi.org/10.1007/s11273-011-9246-y>, 2012.
- 1703 Kelley, D. I., Bistinas, I., Whitley, R., Burton, C., Marthews, T. R., and Dong, N.: How
1704 contemporary bioclimatic and human controls change global fire regimes, *Nat. Clim. Chang.*,
1705 9, 690–696, <https://doi.org/10.1038/s41558-019-0540-7>, 2019.
- 1706 Krawchuk, M. A. and Moritz, M. A.: Constraints on global fire activity vary across a resource
1707 gradient, *Ecology*, 92, 121–132, <https://doi.org/10.1890/09-1843.1>, 2011.
- 1708 Kumar, S., Getirana, A., Libonati, R., Hain, C., Mahanama, S., and Andela, N.: Changes in land
1709 use enhance the sensitivity of tropical ecosystems to fire-climate extremes, *Sci Rep*, 12, 964,
1710 <https://doi.org/10.1038/s41598-022-05130-0>, 2022.
- 1711 Kunst, C. and Bravo, S.: Ecología y régimen de fuego en la región chaqueña argentina, in:
1712 Fuego en los ecosistemas Argentinos, 47–59, 2003.
- 1713 Kunst, C., Bravo, S., Monti, E., Cornacchione, M., and Godoy, J.: El fuego y el manejo de
1714 pasturas naturales y cultivadas de la región chaqueña, *Fuego en los Ecosistemas Argentinos*.
1715 Ediciones INTA, 21, 239–247, 2003.
- 1716 Kunst, C., Navall, M., Ledesma, R., Silberman, J., Anríquez, A., Coria, D., Bravo, S., Gómez,
1717 A., Albanesi, A., Grasso, D., Nuñez, J. A. D., González, A., Tomsic, P., and Godoy, J.:
1718 Silvopastoral Systems in the Western Chaco Region, Argentina, in: *Silvopastoral Systems in*
1719 *Southern South America*, edited by: Peri, P. L., Dube, F., and Varella, A., Springer International
1720 Publishing, Cham, 63–87, https://doi.org/10.1007/978-3-319-24109-8_4, 2016.
- 1721 Kusch, E. and Davy, R.: KrigR – A tool for downloading and statistically downscaling climate
1722 reanalysis data, *Environmental Research Letters*, 17, [https://doi.org/10.1088/1748-](https://doi.org/10.1088/1748-9326/ac48b3)
1723 [9326/ac48b3](https://doi.org/10.1088/1748-9326/ac48b3), 2022.
- 1724 Laurent, P., Mouillot, F., Yue, C., Ciais, P., Moreno, M. V., and Nogueira, J. M. P.: FRY, a
1725 global database of fire patch functional traits derived from space-borne burned area products,
1726 *Sci Data*, 5, 180132, <https://doi.org/10.1038/sdata.2018.132>, 2018.
- 1727 Levers, C., Piquer-Rodríguez, M., Gollnow, F., Baumann, M., Camino, M., Gasparri, N. I.,
1728 Gavier-Pizarro, G. I., le Polain de Waroux, Y., Müller, D., Nori, J., Pötzschner, F., Romero-
1729 Muñoz, A., and Kuemmerle, T.: What is still at stake in the Gran Chaco? Social-ecological
1730 impacts of alternative land-system futures in a global deforestation hotspot, *Environ. Res. Lett.*,
1731 19, 064003, <https://doi.org/10.1088/1748-9326/ad44b6>, 2024.
- 1732 Linley, G. D., Jolly, C. J., Doherty, T. S., Geary, W. L., Armenteras, D., Belcher, C. M., Bliege
1733 Bird, R., Duane, A., Fletcher, M., Giorgis, M. A., Haslem, A., Jones, G. M., Kelly, L. T., Lee,
1734 C. K. F., Nolan, R. H., Parr, C. L., Pausas, J. G., Price, J. N., Regos, A., Ritchie, E. G., Ruffault,
1735 J., Williamson, G. J., Wu, Q., and Nimmo, D. G.: What do you mean, ‘megafire’?, *Global Ecol*
1736 *Biogeogr*, 31, 1906–1922, <https://doi.org/10.1111/geb.13499>, 2022.

- 1737 Lizundia-Loiola, J., Otón, G., Ramo, R., and Chuvieco, E.: A spatio-temporal active-fire
1738 clustering approach for global burned area mapping at 250 m from MODIS data, *Remote*
1739 *Sensing of Environment*, 236, 111493, <https://doi.org/10.1016/j.rse.2019.111493>, 2020.
- 1740 Loto, D. and Bravo, S.: Species composition, structure, and functional traits in Argentine Chaco
1741 forests under two different disturbance histories, *Ecological Indicators*, 113, 106232,
1742 <https://doi.org/10.1016/j.ecolind.2020.106232>, 2020.
- 1743 MacQueen, J.: Some methods for classification and analysis of multivariate observations, in:
1744 *Proceedings of the Fifth Berkeley Symposium on Mathematical Statistics and Probability*,
1745 *Volume 1: Statistics*, 281–298, 1967.
- 1746 Marengo, J., Martinez, R., Tapia, B., Allen, T., Basantes, R., Hernandez-Espinoza, K.,
1747 Alvarado, L., Baddour, O., Ransom, C., Silva, Á., Báez, J., Gomez, F., Costa, F., Avalos, G.,
1748 Estella, J., and Kennedy, J.: State of the Climate in Latin America and the Caribbean 2021
1749 (WMO-No. 1295), 2022.
- 1750 McDaniel, J., Kennard, D., and Fuentes, A.: Smokey the Tapir: Traditional Fire Knowledge
1751 and Fire Prevention Campaigns in Lowland Bolivia, *Society & Natural Resources*, 18, 921–
1752 931, <https://doi.org/10.1080/08941920500248921>, 2005.
- 1753 Meinshausen, N.: Quantile Regression Forests, *Journal of Machine Learning Research*, 7, 983–
1754 999, 2006.
- 1755 Morello, J. H. and Adámoli, J. M.: Las grandes unidades de vegetación y ambiente del Chaco
1756 argentino, 1968.
- 1757 Moreno, M. V., Laurent, P., and Mouillot, F.: Global intercomparison of functional
1758 pyrodiversity from two satellite sensors, *International Journal of Remote Sensing*, 42, 9523–
1759 9541, <https://doi.org/10.1080/01431161.2021.1999529>, 2021.
- 1760 Mouillot, F., Schultz, M. G., Yue, C., Cadule, P., Tansey, K., Ciais, P., and Chuvieco, E.: Ten
1761 years of global burned area products from spaceborne remote sensing—A review: Analysis of
1762 user needs and recommendations for future developments, *International Journal of Applied*
1763 *Earth Observation and Geoinformation*, 26, 64–79, <https://doi.org/10.1016/j.jag.2013.05.014>,
1764 2014.
- 1765 Mouillot, F., Chen, W., Campagnolo, M., and Ciais, P.: FRYv2.0: a global fire patch
1766 morphology database from FireCCI51 and MCD64A1, *Copernicus Meetings*,
1767 <https://doi.org/10.5194/egusphere-egu23-9575>, 2023.
- 1768 Muñoz-Sabater, J., Dutra, E., Agustí-Panareda, A., Albergel, C., Arduini, G., Balsamo, G.,
1769 Boussetta, S., Choulga, M., Harrigan, S., Hersbach, H., Martens, B., Miralles, D. G., Piles, M.,
1770 Rodríguez-Fernández, N. J., Zsoter, E., Buontempo, C., and Thépaut, J.-N.: ERA5-Land: a
1771 state-of-the-art global reanalysis dataset for land applications, *Earth System Science Data*, 13,
1772 4349–4383, <https://doi.org/10.5194/essd-13-4349-2021>, 2021.
- 1773 Musser, K.: Río de la Plata, Wikipedia, 2024.
- 1774 Naumann, G., Podesta, G., Marengo, J., Luterbacher, J., Bavera, D., Acosta, N. J., Arias-
1775 Muñoz, C., Barbosa, P., Cammalleri, C., Cuartas, L. A., De, E. M., De, F. M., De, J. A., Escobar,
1776 C., Fioravanti, G., Giordano, L., Hrast, E. A., Hidalgo, C., Leal, D. M. O. L., Maetens, W.,

- 1777 Magni, D., Masante, D., Mazzeschi, M., Osman, M., Rossi, L., Seluchi, M., De, L. M. S. M.,
 1778 Spennemann, P., Spinoni, J., Toreti, A., and Vera, C.: Extreme and long-term drought in the La
 1779 Plata Basin: event evolution and impact assessment until September 2022,
 1780 <https://doi.org/10.2760/62557>, 2023.
- 1781 Naval Fernández, Albornoz, J., Bellis, L. M., Baldini, C., Arcamone, J., Silveti, L., Álvarez,
 1782 M. P., and Argañaraz, J. P.: Megaincendios 2020 en Córdoba: Incidencia del fuego en áreas de
 1783 valor ecológico y socioeconómico, *Ecol. Austral*, 33, 136–151,
 1784 <https://doi.org/10.25260/EA.23.33.1.0.2120>, 2023.
- 1785 Naval-Fernández, M. C., Elia, M., Giannico, V., Bellis, L. M., Bravo, S. J., and Argañaraz, J.
 1786 P.: The Pyrogeography of the Gran Chaco's Dry Forest: A Comparison of Clustering
 1787 Algorithms and the Scale of Analysis, *Forests*, 16, 1114, <https://doi.org/10.3390/fl6071114>,
 1788 2025.
- 1789 Nori, J., Torres, R., Lescano, J. N., Cordier, J. M., Periago, M. E., and Baldo, D.: Protected
 1790 areas and spatial conservation priorities for endemic vertebrates of the Gran Chaco, one of the
 1791 most threatened ecoregions of the world, *Diversity and Distributions*, 22, 1212–1219,
 1792 <https://doi.org/10.1111/ddi.12497>, 2016.
- 1793 Olson, D. M., Dinerstein, E., Wikramanayake, E. D., Burgess, N. D., Powell, G. V.,
 1794 Underwood, E. C., and Kassem, K. R.: Terrestrial Ecoregions of the World: A New Map of
 1795 Life on Earth A new global map of terrestrial ecoregions provides an innovative tool for
 1796 conserving biodiversity, *BioScience*, 51, 933–938, 2001.
- 1797 Oom, D., Silva, P. C., Bistinas, I., and Pereira, J. M. C.: Highlighting Biome-Specific
 1798 Sensitivity of Fire Size Distributions to Time-Gap Parameter Using a New Algorithm for Fire
 1799 Event Individuation, *Remote Sensing*, 8, 663, <https://doi.org/10.3390/rs8080663>, 2016.
- 1800 Paritsis, J., Landesmann, J. B., Kitzberger, T., Tiribelli, F., Sasal, Y., Quintero, C., Dimarco, R.
 1801 D., Barrios-García, M. N., Iglesias, A. L., Diez, J. P., Sarasola, M., and Nuñez, M. A.: Pine
 1802 Plantations and Invasion Alter Fuel Structure and Potential Fire Behavior in a Patagonian
 1803 Forest-Steppe Ecotone, *Forests*, 9, 117, <https://doi.org/10.3390/f9030117>, 2018.
- 1804 Paudel, J.: Short-run environmental effects of COVID-19: Evidence from forest fires, *World*
 1805 *Development*, 137, 105120, <https://doi.org/10.1016/j.worlddev.2020.105120>, 2021.
- 1806 Pausas, J. G. and Bradstock, R. A.: Fire persistence traits of plants along a productivity and
 1807 disturbance gradient in mediterranean shrublands of south-east Australia, *Global Ecol*
 1808 *Biogeography*, 16, 330–340, <https://doi.org/10.1111/j.1466-8238.2006.00283.x>, 2007.
- 1809 Pettinari, M. L., Lizundia-Loiola, J., and Chuvieco, E.: ESA CCIECV fire disturbance: D4. 2.1
 1810 product user guide—MODIS, version 1.1, 2021.
- 1811 Pielou, E. C.: The measurement of diversity in different types of biological collections, *Journal*
 1812 *of Theoretical Biology*, 13, 131–144, [https://doi.org/10.1016/0022-5193\(66\)90013-0](https://doi.org/10.1016/0022-5193(66)90013-0), 1966.
- 1813 Poulter, B., Freeborn, P., Jolly, W., and Varner, J.: COVID-19 lockdowns drive decline in
 1814 active fires in southeastern United States, *Proceedings of the National Academy of Sciences*,
 1815 118, e2105666118, <https://doi.org/10.1073/pnas.2105666118>, 2021.

- 1816 Redford, K. H., Taber, A., and Simonetti, J. A.: There is More to Biodiversity than the Tropical
1817 Rain Forests, *Conservation Biology*, 4, 328–330, 1990.
- 1818 Ruffault, J. and Mouillot, F.: How a new fire-suppression policy can abruptly reshape the fire-
1819 weather relationship, *Ecosphere*, 6, art199, <https://doi.org/10.1890/ES15-00182.1>, 2015.
- 1820 Ruffault, J. and Mouillot, F.: Contribution of human and biophysical factors to the spatial
1821 distribution of forest fire ignitions and large wildfires in a French Mediterranean region, *Int. J.*
1822 *Wildland Fire*, 26, 498–508, <https://doi.org/10.1071/WF16181>, 2017.
- 1823 Ruffault, J., Moron, V., Trigo, R. M., and Curt, T.: Objective identification of multiple large
1824 fire climatologies: an application to a Mediterranean ecosystem, *Environ. Res. Lett.*, 11,
1825 075006, <https://doi.org/10.1088/1748-9326/11/7/075006>, 2016.
- 1826 Ruffault, J., Curt, T., Moron, V., Trigo, R. M., Mouillot, F., Koutsias, N., Pimont, F., Martin-
1827 StPaul, N., Barbero, R., Dupuy, J.-L., Russo, A., and Belhadj-Khedher, C.: Increased likelihood
1828 of heat-induced large wildfires in the Mediterranean Basin, *Sci Rep*, 10, 13790,
1829 <https://doi.org/10.1038/s41598-020-70069-z>, 2020.
- 1830 San Martín, R.: Fires, land use, and forest loss in the South American Chaco: understanding
1831 the links between fires, climate, ecosystems, and human activity through remote sensing, PhD
1832 Thesis, Université Paris-Saclay, 2024.
- 1833 San Martín, R., Otlé, C., and Sörensson, A.: Fires in the South American Chaco, from dry
1834 forests to wetlands: response to climate depends on land cover, *fire ecol*, 19, 57,
1835 <https://doi.org/10.1186/s42408-023-00212-4>, 2023.
- 1836 Saucedo, G. I. and Kurtz, D. B.: Seasonality and post fire recovery in a wetland dominated
1837 region: Insights from satellite data analysis in northern Argentina, *Remote Sensing*
1838 *Applications: Society and Environment*, 37, 101480,
1839 <https://doi.org/10.1016/j.rsase.2025.101480>, 2025.
- 1840 Schmidt, M. A. and Castilla, M.: La emergencia del fuego en un territorio hidrosocial: incendios
1841 en las provincias de Salta y Chaco, I Encuentro Territorios Hidrosociales en Disputa (ETHIS)
1842 (Chaco, 25 y 26 de agosto de 2022), 2023.
- 1843 Shannon, C. E.: A Mathematical Theory of Communication, *Bell System Technical Journal*,
1844 27, 379–423, <https://doi.org/10.1002/j.1538-7305.1948.tb01338.x>, 1948.
- 1845 Sugiyama, M. S., Mendoza, M., and Carpio, M. B.: Resilience and Recovery in the Dry Chaco:
1846 Ecological Knowledge Encoded in Forager Wildfire Narratives, *Journal of Ethnobiology*, 45,
1847 76–94, <https://doi.org/10.1177/02780771241303896>, 2025.
- 1848 Takacs, S., Schulte to Bühne, H., and Pettorelli, N.: What shapes fire size and spread in African
1849 savannahs?, *Remote Sensing in Ecology and Conservation*, 7, 610–620,
1850 <https://doi.org/10.1002/rse2.212>, 2021.
- 1851 Tálamo, A., Lopez De Casenave, J., Núñez-Regueiro, M., and Caziani, S. M.: Regeneración de
1852 plantas leñosas en el Chaco semiárido argentino: relación con factores bióticos y abióticos en
1853 micrositios creados por el aprovechamiento forestal, *Bosque (Valdivia)*, 34, 13–14,
1854 <https://doi.org/10.4067/S0717-92002013000100007>, 2013.

- 1855 Torrella, S. A. and Adámoli, J.: Situación ambiental de la ecorregión del Chaco Seco, La
1856 situación ambiental Argentina, 75–82, 2005.
- 1857 Van Wagner, C. E.: Development and structure of the Canadian Forest Fire Weather Index
1858 System, Minister of Supply and Services Canada, Ottawa, 37 pp., 1987.
- 1859 Vidal-Riveros, C., Souza-Alonso, P., Bravo, S., Laino, R., and Ngo Bieng, M. A.: A review of
1860 wildfires effects across the Gran Chaco region, *Forest Ecology and Management*, 549, 121432,
1861 <https://doi.org/10.1016/j.foreco.2023.121432>, 2023.
- 1862 Vidal-Riveros, C., Watler Reyes, W. J., Ngo Bieng, M. A., and Souza-Alonso, P.: Assessing
1863 Fire Regimes in the Paraguayan Chaco: Implications for Ecological and Fire Management, *Fire*,
1864 7, 347, <https://doi.org/10.3390/fire7100347>, 2024.
- 1865 Vitolo, C., Di Giuseppe, F., Barnard, C., Coughlan, R., San-Miguel-Ayanz, J., Libertá, G., and
1866 Krzeminski, B.: ERA5-based global meteorological wildfire danger maps, *Sci Data*, 7, 216,
1867 <https://doi.org/10.1038/s41597-020-0554-z>, 2020.
- 1868 Wright, M. N. and Ziegler, A.: ranger: A Fast Implementation of Random Forests for High
1869 Dimensional Data in C++ and R, *Journal of Statistical Software*, 77, 1–17,
1870 <https://doi.org/10.18637/jss.v077.i01>, 2017.
- 1871 Yebra, M., Scortechini, G., Badi, A., Beget, M. E., Boer, M. M., Bradstock, R., Chuvieco, E.,
1872 Danson, F. M., Dennison, P., Resco de Dios, V., Di Bella, C. M., Forsyth, G., Frost, P., Garcia,
1873 M., Hamdi, A., He, B., Jolly, M., Kraaij, T., Martín, M. P., Mouillot, F., Newnham, G., Nolan,
1874 R. H., Pellizzaro, G., Qi, Y., Quan, X., Riaño, D., Roberts, D., Sow, M., and Ustin, S.: Globe-
1875 LFMC, a global plant water status database for vegetation ecophysiology and wildfire
1876 applications, *Sci Data*, 6, 155, <https://doi.org/10.1038/s41597-019-0164-9>, 2019.
- 1877